An attempt to constrain the age, duration, and eruptive history of the Karoo flood basalt: Naude's Nek section (South Africa)

Maud Moulin,[1,2] Frédéric Fluteau,[1,2] Vincent Courtillot,[1,2] Julian Marsh,[3] Guillaume Delpech,[4,5] Xavier Quidelleur,[4,5] Martine Gérard,[6] and Anne E. Jay[7]

Received 7 January 2011; revised 17 March 2011; accepted 7 April 2011; published 13 July 2011.

[1] We have carried out paleomagnetic sampling of a ~750 m sequence of the Karoo large igneous province (Naude's Nek Pass, South Africa). K-Ar dating (Cassignol-Gillot) has been performed on four samples from the 650 m upper unit (mean age 179.2 ± 1.8 Ma) and a sample from the lower unit (184.8 ± 2.6 Ma). A succession of two phases of volcanism is suggested. The lower 25 flows (115 m thick) have recorded a reversed polarity; the next 23 flows (135 m thick) are transitional and contribute a detailed record of the "Van Zijl" (1962) Jurassic reversal. The upper 38 flows (500 m thick) have normal polarity. Directional groups (DGs) of lava flows with quasi-identical remanence directions indicate eruption durations too short to have recorded geomagnetic secular variation and hence are interpreted as single eruptive events. Altogether, 19 DGs and 10 sheet lobes yield a sequence of 29 distinct directions. This could correspond to a total eruptive activity shorter than 3000 years, less than one per mil of the total duration over which the section was emplaced. We obtain a new paleomagnetic pole for South Africa at ~180 Ma (λ = 75.2°N, φ = 276.4°E, A_{95} = 5.8°, N = 19), which is consistent with earlier reports.

Citation: Moulin, M., F. Fluteau, V. Courtillot, J. Marsh, G. Delpech, X. Quidelleur, M. Gérard, and A. E. Jay (2011), An attempt to constrain the age, duration, and eruptive history of the Karoo flood basalt: Naude's Nek section (South Africa), *J. Geophys. Res.*, *116*, B07403, doi:10.1029/2011JB008210.

1. Introduction

[2] Sixteen large igneous provinces (LIPs), either continental flood basalts (CFB) or oceanic plateaus, have been emplaced during the Phanezoic [e.g., *Courtillot and Renne*, 2003]. Despite several decades of research on LIPs, the generation, emplacement and climatic and biotic consequences of these gigantic outpourings of magma are still not fully understood [*Bryan et al.*, 2010]. The ages of LIPs are reasonably well known through numerous geochronological studies. A temporal match between flood basalts and mass extinction events holds over the past 360 Ma [*Rampino and Stothers*, 1988; *Courtillot*, 1994] (see *Courtillot and Renne* [2003] for a recent review). The correlation, which extended at first only back to the Permo-Triassic (PT) extinctions, has more recently been extended to include the Guadalupian-Tatarian boundary at about 260 Ma [*Wignall et al.*, 2009] and more tentatively the Frasnian-Famennian boundary around 360 Ma [*Kravchinsky et al.*, 2002; *Courtillot et al.*, 2010]. Though *Thiede and Vasconcelos* [2010] have recently questioned the synchronism of volcanism in the case of the Parana CFB and Jurassic-Cretaceous extinction event, temporal coincidence between volcanism and mass extinctions (given the precision of most current radiometric ages, which is on the order of 1% at best; see, e.g., the discussion in the work of *Chenet et al.* [2007]) remains widely accepted.

[3] One needs to understand the mechanisms by which mass extinctions and volcanism are linked. Two major processes are suggested: a direct effect driven by the release of volcanic gases into the atmosphere [e.g., *Wignall*, 2001; *Courtillot and Renne*, 2003; *Chenet et al.*, 2009] and an indirect effect due to degassing induced by contact metamorphism in case LIP feeders are intruded in sedimentary deposits [*Svensen et al.*, 2004, 2007; *Ganino and Arndt*, 2009]. However, details of the atmospheric and biotic consequences of gas release from flood basalt volcanism remain poorly understood. Taking into account the average concentration of sulfur (about 1000 ppm) and CO_2 (0.5%) in basaltic magmas [*Self et al.*, 2006], one can estimate the total release of SO_2 at about 6 Tt (teraton) and CO_2 at about 14 Tt per million km^3 of basalt during LIP emplacement [*Chenet et al.*, 2009]. Degassing induced when hot magmas intrude C- or S-rich sedimentary layers (dolomite, evaporite, organic carbon-rich layer, carbonate, coal for C; anhydrite, gypsum for S) could be larger than that degassed from magma itself [*Ganino and Arndt*, 2009].

[1]Equipe de Paléomagnétisme, Institut de Physique du Globe, UMR 7154, Sorbonne Paris Cité, Paris, France.
[2]Sciences de la Terre, de l'Environnement et des Planètes, Université Paris Diderot, Sorbonne Paris Cité, Paris, France.
[3]Department of Geology, Rhodes University, Grahamstown, South Africa.
[4]Laboratoire IDES, UMR 8148, Université Paris-Sud, Paris, France.
[5]CNRS, Orsay, France.
[6]IMPMC, IRD, UMR 7590, UPMC, IPGP, CNRS, Paris, France.
[7]Department of Earth Science and Engineering, Imperial College, London, UK.

0148-0227/11/2011JB008210

[4] Understanding the effects of LIP emplacement on climate and environment requires knowledge of injection history and rates. The total duration of LIP emplacement has long been determined using radiochronometric methods and magnetostratigraphy. Many studies underline the brevity of LIP emplacement, on the order of 1 Myr. More precisely, magmatism may have lasted 2–4 Myr in the Deccan traps [*Jerram and Widdowson*, 2005; *Chenet et al.*, 2007], 6–10 Myr in the Siberian [*Ivanov et al.*, 2005] and Parana-Etendeka [*Thompson et al.*, 2001] traps, and 4 ± 1 Myr for the emplacement of the main part of the Karoo traps [*Jourdan et al.*, 2008]. If volcanism and gas injection in the atmosphere had taken place uniformly over such durations, one might have doubts on the ability of LIP emplacement to cause severe climatic change and biotic crises [*Jourdan et al.*, 2005]. But recent studies have revealed the intermittent character of flood basalt volcanism [*Knight et al.*, 2004; *Riisager et al.*, 2003; *Riley et al.*, 2006; *Chenet et al.*, 2008, 2009]. For instance, *Chenet et al.* [2008, 2009] have shown that the Main Province of the Deccan traps (~80% of the volume of basalt) was erupted in ~30 major single eruptive events (SEEs) with typical volumes ranging from 1000 to 20,000 km^3 and ~40 smaller individual lava units of about 1,000 km^3 or less.

[5] SEEs are identified after paleomagnetic analysis: they consist of one or several lava flows that display the same characteristic remanent magnetization and which have therefore failed to record significant secular variation of the Earth's magnetic field. Under the hypothesis that the speed and amplitude of secular variation at the time of eruption were similar to those recorded in recent millennia by archeomagnetic analysis [e.g., *Gallet et al.*, 2003], this implies rapid emplacement of the lava over a period not exceeding 100 years, and perhaps as short as a decade. In the case of the Main Province of the Deccan traps, *Chenet et al.* [2009] concluded that the total time of emission of all combined SEEs could have been (much) less than 10 ka within the ~1 to 2 Myr long period of extrusion recorded by geochronology, stratigraphy and paleontology. Single eruptive events are not restricted to the Deccan traps: they have also been identified in the Central Atlantic Magmatic Province [*Knight et al.*, 2004] and Siberian traps [*Pavlov et al.*, 2010]. During eruption of these SEEs, eruption rates could have been 2 to 3 orders of magnitude larger than if volcanism had been uniformly spread over the whole duration of CFB formation.

[6] In the present contribution, we apply the same methods that were successful in defining the time of the Deccan volcanic pulses [*Chenet et al.*, 2007, 2008, 2009] to the Karoo (or Karoo-Ferrar) magmatic province, which is considered as one of the largest outpourings of basaltic magmas during the Phanerozoic, yet is apparently associated with a rather minor extinction event, compared to the PT/Siberian trap or Cretaceous-Tertiary (KT)/Deccan trap pairs of events [e.g., *Pálfy and Smith*, 2000]. The Karoo province consists of a complex series of separate lava flow outcrops over (and within) much of southern Africa (Figures 1a and 1b). The southern African part of the Karoo consists of a lava flow plateau (i.e., a true CFB), exposed mainly in Lesotho, a sill and dike system extending over much of the sedimentary Karoo Basin, and extensive lava flow outcrops in Namibia, Botswana, Zimbabwe and Mozambique, including the radiating Lebombo, Tuli and Save-Mwenezi volcanic ranges, which is reminiscent of a rift-rift-rift (RRR) triple junction. Extensive lava flows are also found below the sands of the Kalahari desert [*Green*, 1966]. The Ferrar province, which extends all the way to Tasmania and New Zealand, forms an elongated extension of the Karoo in Antarctica (Figure 1a). The main part of the combined Karoo-Ferrar volcanic province was erupted within a 4 ± 1 Myr period centered at about 182 Ma [*Encarnacion et al.*, 1996; *Duncan et al.*, 1997; *Riley and Knight*, 2001; *Jourdan et al.*, 2008].

[7] This age matches the late Pliensbachian–Early Toarcian biotic crisis, a second-order mass extinction divided into at least two phases: the Pliensbachian-Toarcian boundary and an early Toarcian event [*Little*, 1996; *Cecca and Macchioni*, 2004; *Wignall and Bond*, 2008]. About 5% of marine species in both Pliensbachian and Toarcian and ~2 to 13% of terrestrial biota in the Toarcian became extinct [*Little and Benton*, 1995]. The crisis is coeval with a number of environmental perturbations, including widespread marine anoxia and changes in temperatures and hydrological cycles [*Jenkyns*, 1988; *Cohen et al.*, 2004; *McElwain et al.*, 2005]. Two negative $\delta^{13}C$ excursions, a first one during the Late Pliensbachian and a second one during the Early Toarcian, have been linked to two successive injections of ^{13}C-depleted carbon into the atmosphere-ocean reservoirs [*Hesselbo et al.*, 2000; *Suan et al.*, 2008; *Hermoso et al.*, 2009]. Although the environmental effects of massive volcanism are far from being fully understood, it has been suggested that the emplacement of the Karoo-Ferrar traps played a role in the environmental perturbations, oceanic anoxia events and marine and terrestrial extinctions observed during the Late Pliensbachian and Early Toarcian [*Pálfy and Smith*, 2000; *Suan et al.*, 2010].

[8] We have undertaken a detailed paleomagnetic and geochronologic study of the Lesotho part of the Karoo traps, starting with the 700 m thick Naude's Nek section in the Eastern Cape province of South Africa, in which the lower part of the Karoo traps is exposed [*Marsh et al.*, 1997]. We have followed the procedure developed for the Deccan traps [*Chenet et al.*, 2007, 2008, 2009] in an attempt to resolve the detailed timing of the eruptive sequence, and specifically to identify whether large SEEs and volcanic pulses were present. A geological description of the section and its surroundings is given in section 2 of this paper. The geochronologic methods and results are given in section 3. The paleomagnetic methods and results are given in section 4, including a magnetostratigraphy of the lava pile and the identification of directional groups that serve to define SEEs. A discussion of the reversal test and the determination of a virtual geomagnetic pole for the time of trap emplacement are also given in that section. Section 5 provides a discussion of the number of phases and total duration of Karoo magmatism and some concluding remarks.

2. Geological Setting

2.1. Karoo and Ferrar Lava Outcrops

[9] Widespread volcanic activity occurred throughout southern Africa during the Lower Jurassic, mainly in the Pliensbachian and Toarcian, forming the Karoo province [*Duncan et al.*, 1997; *Riley and Knight*, 2001]. Remnants of

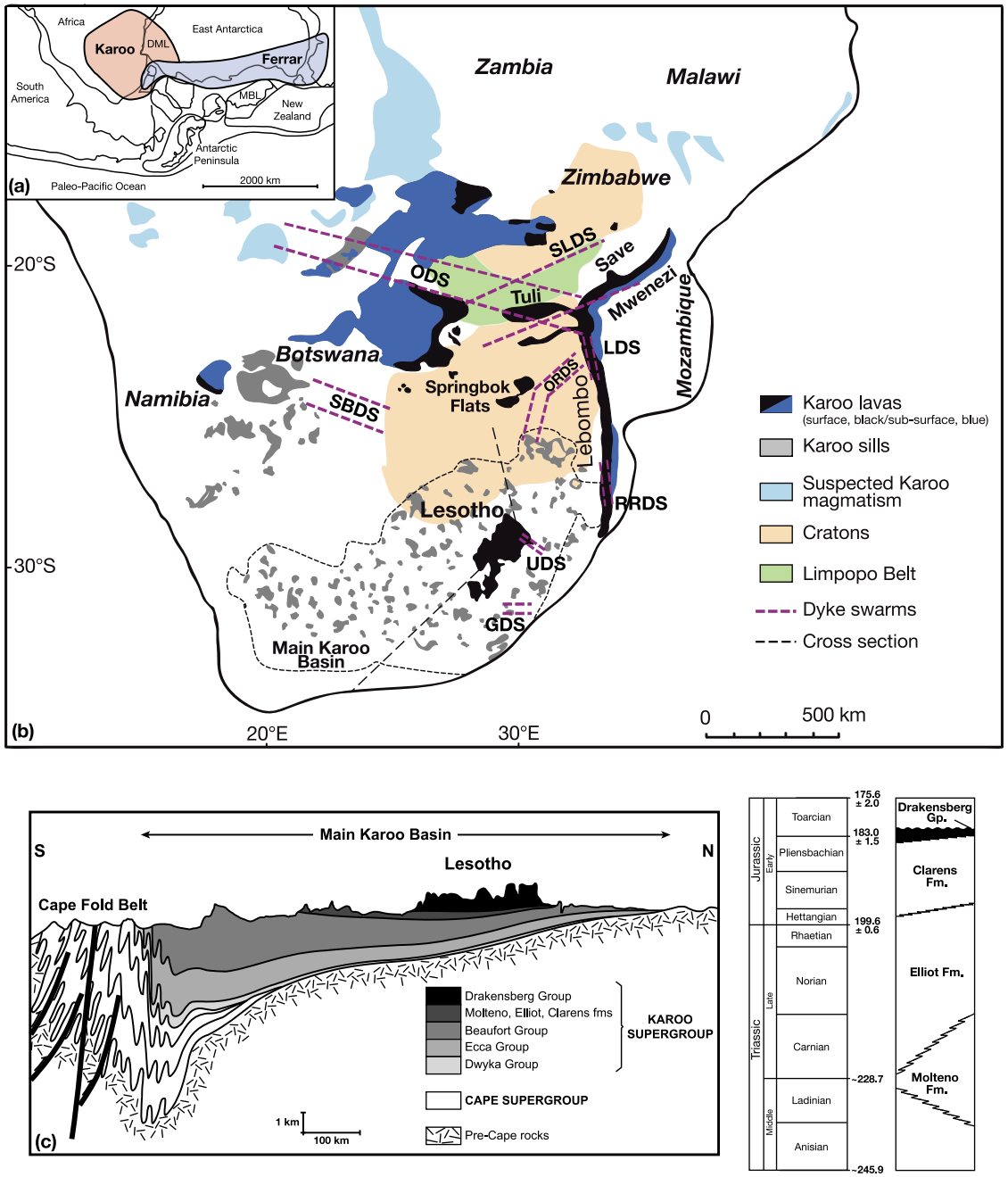

Figure 1. (a) Prebreakup Gondwana reconstruction (~182 Ma) showing major magmatic provinces of Karoo and Ferrar (modified after *Riley and Knight* [2001]). MBL, Marie Byrd Land; DML, Dronning Maud Land. (b) Geological extent of the Karoo large igneous province in southern Africa (modified after *Jourdan et al.* [2008] and *Marsh et al.* [1997, 2003]). ODS, Okavango dike swarm; SLDS, Save Limpopo dike swarm; LDS, Lebombo dike swarm; ORDS, Olifants River dike swarm; RRDS, Rooi Rand dike swarm; SBDS, south Bostwana dike swarm; UDS, Underberg dike swarm; and GDS, Gap dike swarm. The dashed line encloses the Main Karoo Basin [after *Johnson et al.*, 1997]. (c) Cross section of the Main Karoo Basin (modified after *Johnson et al.* [1997]). The location of the cross section (dashed line) is shown in Figure 1b. Stratigraphy of the upper formations of the Karoo Supergroup is modified from *Holzforster* [2007] and *Knoll* [2005]. Geological timescale from *Ogg et al.* [2008].

this magmatic province are represented by volcanic formations resting on the Karoo Supergroup, a stable intracratonic sedimentary basin deposited between Permo-Carboniferous and Early Jurassic times [*Smith et al.*, 1998]. Volcanic remnants are characterized by numerous isolated outcrops [*Eales et al.*, 1984] (Figure 1b). The thickest volcanic sequence (about 1600 m) is found in the Lesotho remnant where it is formally known as the Drakensberg Group (Figure 2). The other main remnants of the Karoo province outcrop in the northern part of South Africa (Springbok Flats), in Namibia

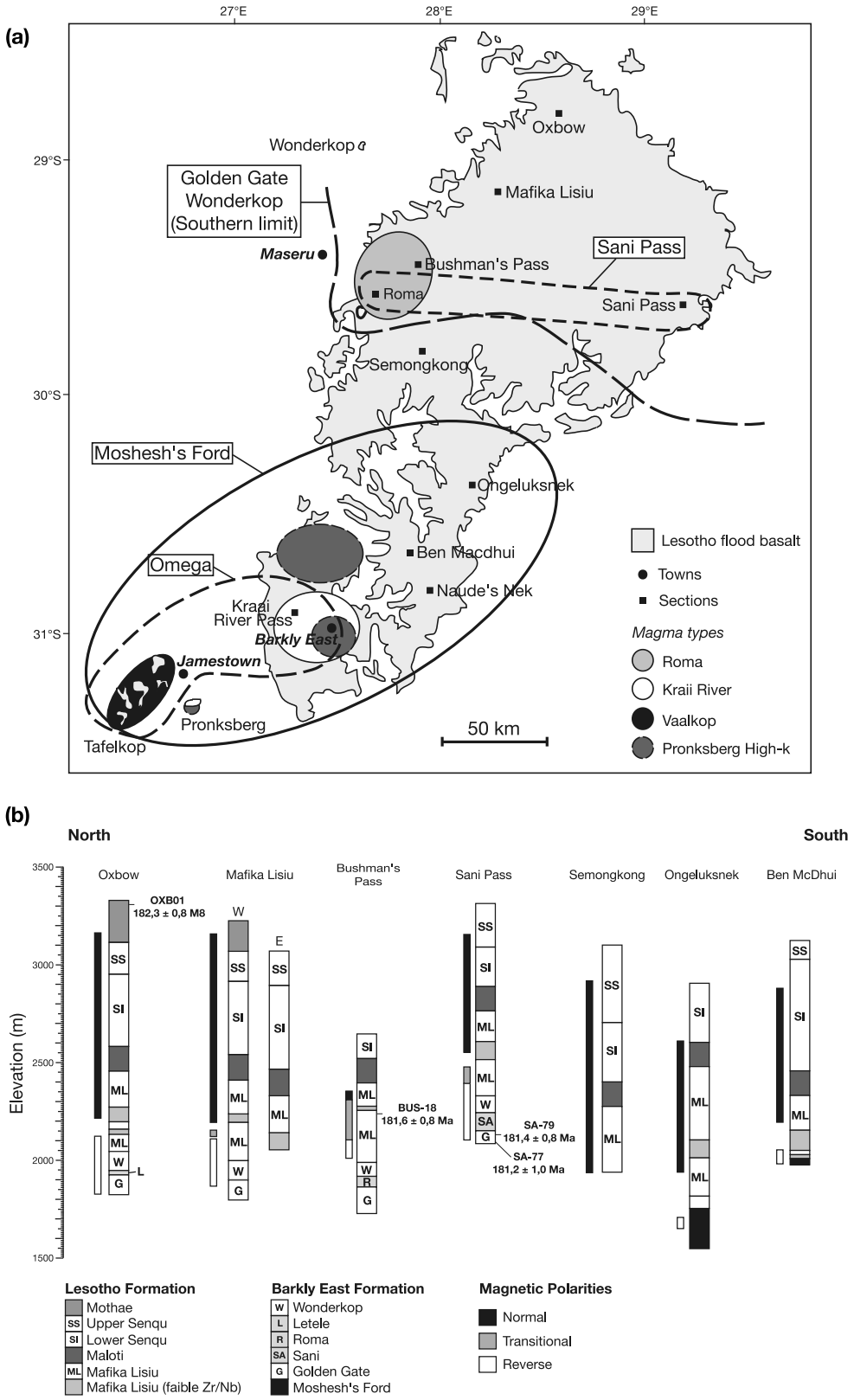

Figure 2. (a) Distribution of the Karoo flood basalt magma types in the Lesotho remnant (modified from *McClintock et al.* [2008], *Marsh and Eales* [1984], *Marsh et al.* [1997], and *Mitchell et al.* [1996]). (b) Geochemical stratigraphy, magnetic stratigraphy, and absolute ages of the Lesotho remnant. Geochemical magma types (units) shown in Figure 2a are from *Marsh et al.* [1997]. Magnetic polarities are from *Rehacek* [1995], *Kosterov and Perrin* [1996], and *Prévot et al.* [2003]. Absolute ages with 1 σ total uncertainties are from *Jourdan et al.* [2007b].

(Hardap Formation, Kalkrand Formation), in Swaziland and on the borders between Zimbabwe and South Africa to the north and between Mozambique and South Africa to the southeast (Lebombo monocline). Rock types are overwhelmingly basalts with almost indistinguishable tholeiitic compositions, but locally other types (andesites, nephelinite, picrite, rhyolites) may be encountered, mainly within the Lebombo monocline [*Eales et al.*, 1984; *Marsh et al.*, 1997]. Erosion of Karoo lava flows reveals a widespread network of doleritic dykes and sills across the whole of southern Africa [*Chevallier and Woodford*, 1999]. Dykes and giant dyke swarms intrude the sedimentary formations of the Karoo Supergroup to the south (South Africa), and the Archean basement to the north (Zimbabwe) [*Eales et al.*, 1984; *Le Gall et al.*, 2002] (Figure 1b).

[10] The Dronning Maud Land magmatic province in Antarctica, which is now separated from the African continent by the southwest Indian Ocean, consists of dykes, sills and basaltic flows [*Harris et al.*, 1990]. Similarities in geochemical signature suggest that this province is related to the Karoo province. Elsewhere, other volcanic units are encountered in Antarctica [*Mitchell et al.*, 1999], but also in the Falkland Islands [*Harris et al.*, 1990; *Le Gall et al.*, 2002; *Riley et al.*, 2005], in Tasmania [*Hergt et al.*, 1989], in the southeastern part of Australia [*Hergt et al.*, 1991] and as far as New Zealand [*Mortimer et al.*, 1995] (Figure 1a). These volcanic units form the Ferrar magmatic province, which was mainly emplaced prior to breakup of Gondwana, in the Early Jurassic [*Riley and Knight*, 2001]. The most voluminous outcrops are located in Antarctica and consist of the mafic layered intrusion of the Dufek Massif, the Ferrar dolerite sills and the Kirkpatrick basalt. Contemporaneous age and close geochemical similarities between the Ferrar dolerites and the low-Ti tholeiitic basalts of the Karoo province support a common origin for the two provinces [*Duncan et al.*, 1997; *Elliot and Fleming*, 2000; *Riley and Knight*, 2001]. It has been suggested that a thermal anomaly centered below the Weddell Sea may explain Karoo-Ferrar volcanism [*Elliot and Fleming*, 2000; *Storey et al.*, 2001]. The original volume of the Karoo-Ferrar magmatic province is estimated at about ~2.5×10^6 km^3 [*Cox*, 1988; *Encarnacion et al.*, 1996], making it one of the largest magmatic provinces erupted during the Phanerozoic.

[11] The area has been witness to a long magmatic history, lasting some 30 Myr, starting with emplacement of the Karoo-Ferrar large igneous province and ending with the onset of ocean crust formation in the Indian Ocean [*Jourdan et al.*, 2006]. The main magmatic (basaltic) episode of the Karoo traps occurred essentially over a 4 ± 1 Myr period [*Duncan et al.*, 1997; *Jourdan et al.*, 2007b, 2008], initially estimated at around 183 Myr by *Duncan et al.* [1997]. More recently, *Jourdan et al.* [2007b, 2008] have shown that magmatic activity climaxed essentially around 180 Myr. The Ferrar province has yielded an age of 182 ± 2 Ma, confirming that its emplacement was coeval with that of the Karoo province [*Kyle et al.*, 1981; *Encarnacion et al.*, 1996; *Riley and Knight*, 2001].

2.2. Naude's Nek Section

[12] This study focuses on the low-Ti tholeiitic basalts that form the lower part of the Drakensberg group in the southern Lesotho remnant. The lavas (Figure 2) rest on an aeolian sandstone unit, the Clarens Formation, which represents the last detrital unit of the Karoo Supergroup [*Johnson et al.*, 1996] (Figure 1c). The Clarens Formation resulted from successive episodes of aridity, ephemeral streams and playa lakes [*Smith*, 1990, 1993; *Bordy and Catuneanu*, 2002]. The section we studied is located between the small town of Rhodes (1500 m altitude) and Naude's Nek Pass (2500 m altitude) in the Eastern Cape Province (South Africa; Figure 2a). Two geochemical units are encountered: a lower one, ~100 m thick, named Moshesh's Ford (within the Barkly East Formation) and an upper unit, 650 m thick, named Mafika Lisiu (within the Lesotho Formation, Figure 2) [*Marsh and Eales*, 1984; *Marsh et al.*, 1997]. The Barkly East Formation consists of thin discrete and heterogeneous geochemical units extending over small areas (Figure 2). In the northern part of the Lesotho volcanic pile (north of about 30°S), the Barkly East Formation is subdivided into six geochemical units, in which the Moshesh's Ford unit does not occur. The latter is only found in the southern part of the Lesotho magmatic province (south of about 30°S). The Mafika Lisiu unit is encountered over the whole Lesotho magmatic province [*Marsh et al.*, 1997]. Indeed, the Lesotho Formation comprises thicker chemical units, less variable in composition, sprawling over the entire volcanic province (Figure 2b). Thus the Naude's Nek section gives access to the onset of volcanism but not to the last eruptive events. The highest lava flows emplaced during the last stage of volcanism are located about 800 m above the altitude of Naude's Nek Pass (2550 m) farther north in Lesotho (e.g., near Oxbow; see Figure 2).

[13] In order to determine the sampling strategy for paleomagnetic studies, we have constructed a log of the whole section (Figure 3). The main volcanic features and types, the style and boundaries of flows, and the petrology have been noted, following *Self et al.* [1997] and *Thordarson and Self* [1998] [see also *Guilbaud et al.*, 2005], who define a *flow field* as an aggregate of lava units, a *lava flow* as a result of a single outpouring of lava, and a *flow lobe* as a single lava unit bounded by a glassy rind or selvage. As is common in traps, a large-scale flow lobe (wider than 10^2 to 10^3 m) is called a sheet flow lobe (shortened to *sheet lobe*). A flow lobe is further characterized by a basal crust with moderate vesicularity (less than 10% of the total thickness) comprising pipe vesicles, a lava core (40–60% of the total thickness) with low vesicularity, except for the presence of sparse megavesicles, vesicle cylinders or horizontal vesicular sheets (HVS), and a surface crust (40–50% of the total thickness) which is highly vesicular. In the field, we have identified lava units on the basis of the occurrence of pipe vesicles in what is interpreted as the basal crust of an upper lava unit, overlying vesicles in the surface crust of a lower lava unit (Figure 3). Their thickness varies from ~10^{-1} m to ~20 m. Because lava flows may be either composed of a single flow lobe or of several lobes erupted simultaneously, we cannot easily distinguish lava flows from flow lobes, at least in a systematic way. Two lava flows can occasionally be separated by a red weathered horizon and/or a sedimentary layer (Figure 3).

[14] We have sampled all identified flow lobes for paleomagnetism and selected the less weathered ones for dating along the Naude's Nek road for the upper sites and in the bed of the Bell River (BR traverse) for the lower sites (NN02 to NN47, ND48 to ND66 and NC01 to NC07),

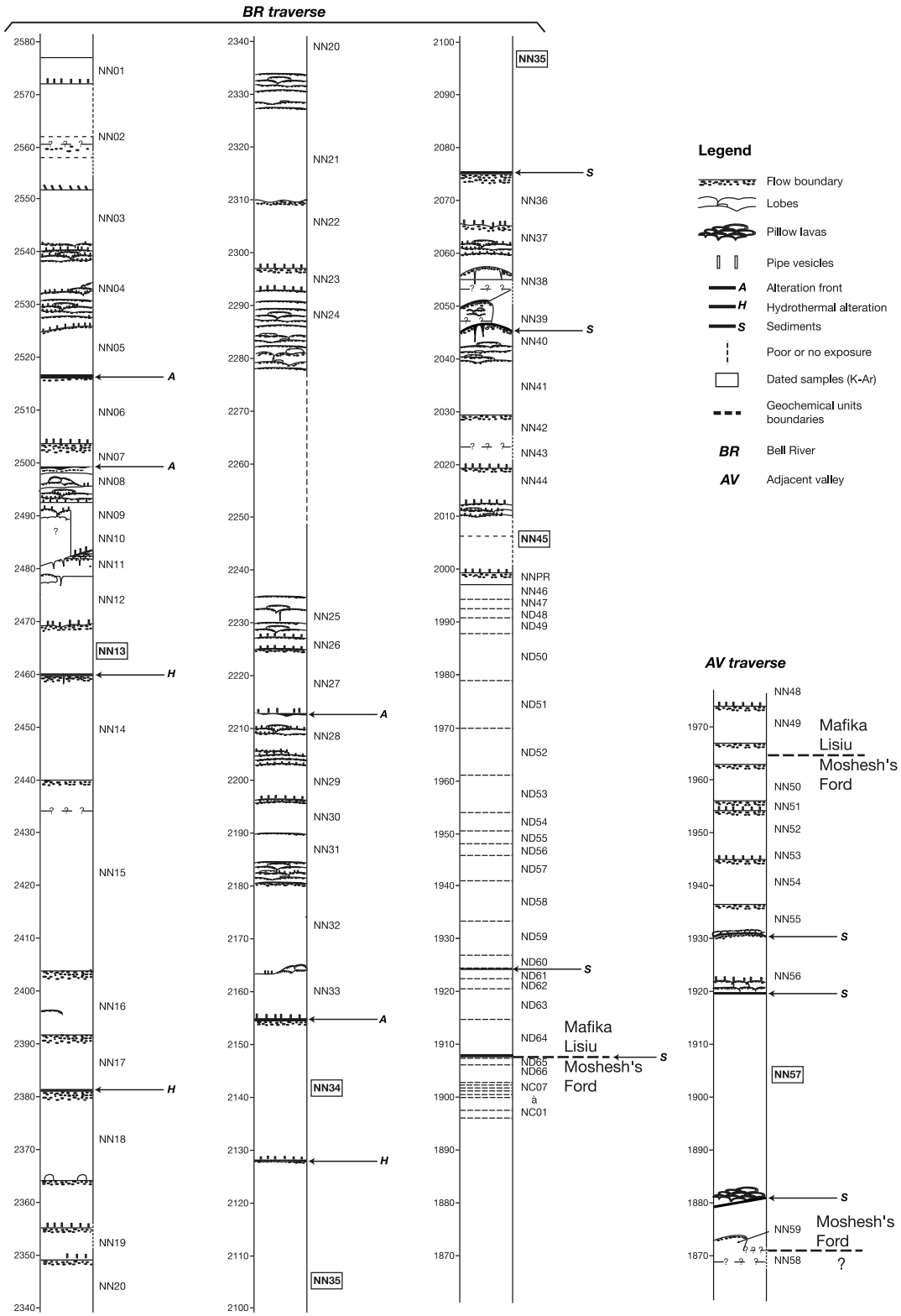

Figure 3. Stratigraphic log of the Naude's Nek section: main (BR) traverse and adjacent small valley (AV) traverse.

except for sites NN48 to NN59 which were sampled in a small adjacent stream (AV traverse) (Figures 3 and 4). The total thickness of these traverses reaches 790 m, with an overlap of about 100 m (see also Figure 9). The lower part of the section is a composite and we analyze the Bell River (BR) traverse and the adjacent small valley (AV) traverse (~110 m thick) separately. The boundary between the Moshesh's Ford and Mafika Lisiu units is located at an

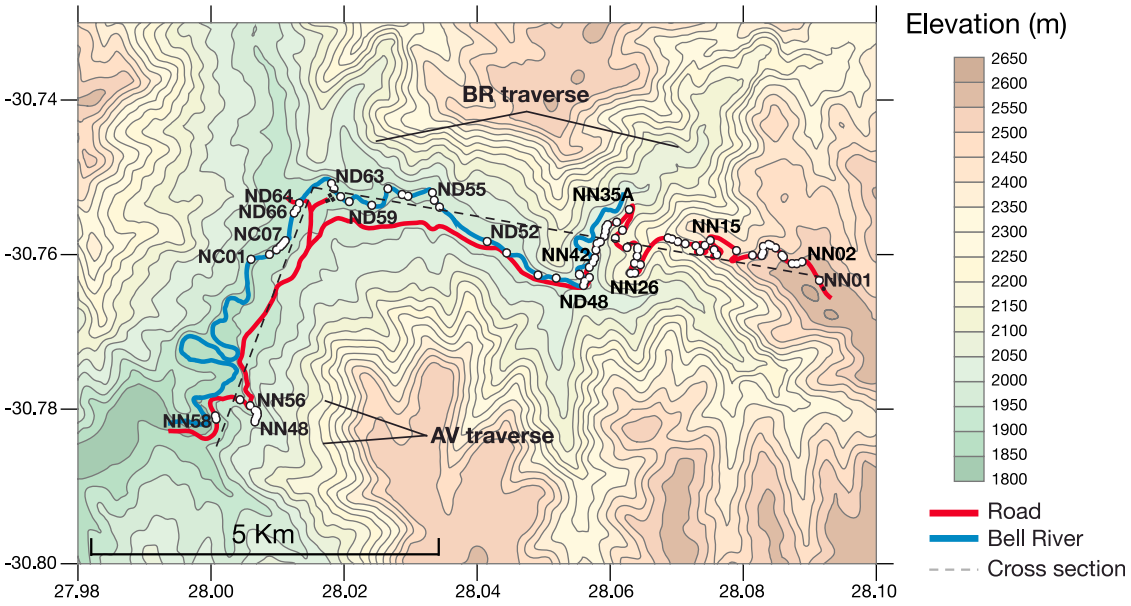

Figure 4. Location of the 88 paleomagnetic sites sampled along the BR and AV traverses. Topographic map is based on Shuttle Radar Topography Mission 2 (SRTM2) [*Rodriguez et al.*, 2005].

elevation of 1908 m in the BR traverse (between sites ND64 and ND65, Figure 3). In the AV traverse, sites located below an elevation of 1935 m (sites NN55 to NN59) belong to the Moshesh's Ford geochemical unit, except site NN58, which belongs to an undefined geochemical unit. The boundary could not be determined in the AV traverse since we do not have complete geochemical data for these sites. However, paleomagnetic analyses provide us with an estimate of its location (see below). Eighteen paleomagnetic sites were drilled in the Moshesh's Ford unit, 9 in the AV traverse (~100 m thick section) and 9 in the BR traverse (~10 m thick section), and 69 in the Mafika Lisu unit.

[15] At the bottom of the section, the contact between the Clarens sandstone and the Karoo basalt is clearly visible a few meters below the lowest paleomagnetic site (NN58, 1865 m) in the AV traverse. The top of the Clarens Formation presents a smooth topography, not exceeding a few tens of meters at a regional scale, indicating that the first lava flows were emplaced on an irregular but flattish paleosurface. The first outcropping lava flow belongs to an undetermined geochemical unit below the Moshesh's Ford unit. The number of sites within the small thickness of the Moshesh's Ford unit in the BR traverse is due to the presence of several thin flow lobes. In this unit, we encountered some peculiar volcanic features such as pillow lavas, already mentioned in other localities in this area [*Lock et al.*, 1974; *Marsh and Eales*, 1984] (Figure 3), and likely due to the outpouring of magma in local lakes.

[16] Seven indurate sedimentary layers, sometimes baked over ~10 cm by the overlying lava flows, are observed in the lower part of the section between 1880 m and 2075 m elevations (Figure 3). The thickness of these layers ranges from a few tens of centimeters to about 1–2 m. The thickest deposit reaches 4 m at 2075 m. These interbedded sedimentary layers are clearly linked to the Clarens Formation: they consist essentially of quartzite rich clayey siltstones with minor amounts of volcanodetritic minerals (feldspars, pyroxene). Among the minor detrital minerals, smectite and zeolite occurrences provide evidence of erosion of altered basalts as well. A lacustrine playa origin for these deposits is likely. The altered bases of overlying flows and the thin baked sediments attest to emplacement of lava in partially humid conditions. Quartzite occurrence suggests that part of the huge sedimentary Karoo Basin was not yet entirely covered by lava flows at that time. The presence of sediment layers testifies to periods of quiescence [*Lock et al.*, 1974] (Figure 3), for which we have no estimate of duration. However, minerals from the weathered lower lava flows included within the sedimentary layers suggest a time of quiescence long enough to promote weathering; all lower flows covered by sediments are strongly altered. The paragenesis of the saprolite facies of the lower flows is essentially smectite-zeolite-feldspar-pyroxene.

[17] There is no significant occurrence of sediment layers above 2075 m in the Naude's Nek section, that is, about 200 m above the top of the Clarens Formation. This may reflect the time after which most of the Karoo Basin was nearly covered by lava flows, or decreasing intervals between volcanic pulses. Four red weathered horizons and three hydrothermalized lava contacts, between 2128 m and 2517 m (Figure 3), have been observed along the section. All of these appear within lava lobe structures which have been more affected by hydrothermal fluids or by topographic irregularities; these lava lobe structures are more easily altered. Some of them have been affected by more recent weathering or metamorphism (lava bowl features and chlorite occurrence). The more mature alteration fronts are characterized by a basaltic saprolite covered by orange to red smectite and hematite rich horizons, a few centimeters thick, suggesting paleosols. At 2213 m, two red horizons display a paragenesis with quartz, smectite, zeolite, hematite and minor feldspar

and pyroxene. The silty quartz suggests either a colluvional paleosol or the last occurrence of lacustrine deposits.

3. Dating of the Naude's Nek Section

3.1. Previous Results

[18] Lithostratigraphic correlation of the Clarens Formation with other basins is very difficult; biostratigraphic correlation is based on reptile fossils but time resolution is not very accurate [*Smith*, 1993]. On the basis of tetrapod fossil records, the lowest horizon of the Clarens formation appears to be Sinemurian [*Knoll*, 2005]. The oldest magmatic events of the Karoo traps are dated at about 184 Ma, suggesting that the first stage of volcanism occurred during the Pliensbachian, in agreement with the age of the uppermost level of the Clarens formation deduced from biostratigraphy. (The age of the Pliensbachian-Toarcian boundary is estimated at 183.0 ± 0.8 Ma [*Gradstein et al.*, 2004]; the uncertainty is likely underestimated.)

[19] The number of available age determinations has significantly increased over the past few years [*Encarnacion et al.*, 1996; *Duncan et al.*, 1997; *Jones et al.*, 2001; *Le Gall et al.*, 2002; *Jourdan et al.*, 2004, 2005, 2007a, 2007b, 2008; *Riley et al.*, 2004, 2006], leading to the conclusion that Karoo activity was concentrated at c.a. 180 Ma. In order to allow intercomparison, all $^{40}Ar/^{39}Ar$ ages described below have been calculated relative to the FCT-sanidine age of 28.02 Ma [*Renne et al.*, 1998], except when specified. All uncertainties quoted herein are given at the 1σ level. The recent data suggest that magmatic activity occurred essentially over a 4 ± 1 Myr period [*Jourdan et al.*, 2007b, 2008]. Within that period, brief (~1 Myr or less), temporally distinct events have been identified [*Jourdan et al.*, 2007b]: the Okavango dyke swarm (179.2 ± 0.2 Ma), the 800 m thick southern Botswana lava pile (178.6 ± 0.3 Ma) and the Lesotho lava pile (181.6 ± 0.4 Ma). Therefore, volcanic activity for the entire province could have lasted as long as 8–10 Ma [*Jourdan et al.*, 2007b], with emplacement of late stage silicic magmatism (from 178 to 174 Ma) followed by intrusion of the MORB-like Rooi Rand dikes [e.g., *Duncan et al.*, 1990], forecasting the onset of oceanic crust formation.

[20] Focusing on the Lesotho remnant, several age determinations have been obtained using the $^{40}Ar/^{39}Ar$ incremental heating technique on whole rock samples [*Duncan et al.*, 1997]. The lack of mineral separation in this procedure leads to rather uncertain age determinations that have been the subject of criticism, which we share [e.g., *Hofmann et al.*, 2000; *Jourdan et al.*, 2007b]. In order to avoid any bias induced by ^{39}Ar recoil in the interstitial glass, we wish to rely only on $^{40}Ar/^{39}Ar$ ages obtained on mineral separates. Only six rock samples from the Lesotho remnant have previously been analyzed by this approach. *Duncan et al.* [1997] obtained an age plateau of 183.9 ± 0.7 Ma on plagioclase (sample KF-10) collected in the lower part of the Barkly East formation, within the Omega unit which overlies Moshesh's Ford basalts in the Kraai River pass some 60 km W of Naude's Nek (Figure 2). The KF-10 mean age was not calculated with the FCT-san age of 28.02 Ma [*Renne et al.*, 1998] and requires recalibrating (see section 6).

[21] *Jourdan et al.* [2007b] took a large number of samples from the Lesotho province. Three of their samples had already been dated by *Duncan et al.* [1997], but on whole rocks: they are the lowermost flow of the Roma section (ROM-01), one flow in the middle part of the Bushman's Pass section (BUS-18), and the highest flow of the Oxbow section (OXB-01). Two additional flows were collected in the lower part of the Sani Pass section (SA77, just above the Clarens formation, and SA79). The $^{40}Ar/^{39}Ar$ plateau ages range from 182.3 ± 0.8 Ma to 181.0 ± 1.0 Ma. Using these results in an age probability density distribution diagram (PDD) (without the J-value error), they suggested a maximum duration of ~0.8 Ma for the emplacement of the whole Lesotho remnant. These ages are slightly younger than the age obtained by *Duncan et al.* [1997], which does not overlap the weighted mean age of 181.6 ± 0.4 Ma [*Jourdan et al.*, 2007b]; these authors propose a cryptic excess $^{40}Ar^*$ and/or standard heterogeneity (FCT-3 biotite) to explain the slight age difference between their results and the age obtained by *Duncan et al.* [1997]. This short duration is consistent with the fact that a single magnetic reversal has been found in the Lesotho sequence [*Van Zijl et al.*, 1962a; *Kosterov and Perrin*, 1996; *Hargraves et al.*, 1997; *Prévot et al.*, 2003] (Figure 2b and section 4 of this paper), despite rather frequent reversals during the Early Jurassic [e.g., *Ogg and Smith*, 2004].

3.2. K-Ar Dating Procedure

[22] K/Ar dating was performed in the Geochronology laboratory at the University of Paris-Sud (Orsay, France), using the nonconventional Cassignol-Gillot K-Ar technique [*Cassignol and Gillot*, 1982; *Gillot and Cornette*, 1986]. About 10 lava flows were sampled in the Naude's Nek section, evenly distributed throughout the section and as little weathered as possible (Figures 2 and 3). Microtextures in the basalts are essentially intersertal and the matrix is composed of plagioclase, clinopyroxene, Fe-Ti oxides with only minor olivine. Plagioclase sometimes occurs as rare phenocrysts. In some samples, the microtexture locally varies to subophitic, with the clinopyroxene enclosing plagioclase microlites of the matrix. Most samples display secondary minerals indicative of an incipient alteration, such as chlorites, serpentine, or partly devitrified glass. Zeolites and few carbonates are present in one sample. A careful petrographic study of thin sections allowed us to select five samples with optically unaltered plagioclase microlites for K/Ar dating. Samples were crushed and separated into different size fractions depending on the plagioclase microlite size distribution and content. Samples without phenocrysts were crushed and sieved in the 100–200 μm size range and heavy liquids were used to isolate plagioclase microlites. The sample containing both plagioclase microlites and phenocrysts (NN57-m) was crushed in order to isolate each fraction. Heavy liquids were used to separate phenocrysts in the 500–1000 μm size fraction and the remainder was crushed in the 125–250 μm size range. Heavy liquids were also used to separate the plagioclase microlites from the groundmass.

[23] The crushed fractions were first cleaned with deionized water, then in an ultrasonic bath for 15 min using a 5% nitric or acetic acid solution in order to remove possible traces of weathered material. Plagioclase microlites were separated from the groundmass using heavy liquids (bromoform, $CHBr_3$) within a narrow density range between 2.66 and 2.74 $g.cm^{-3}$. A Frantz magnetic separator was

finally used to remove the remaining groundmass after heavy liquid density separation. Once pure plagioclase crystals were separated, the K content was measured by atomic absorption spectrometry by measuring a calibration curve between 1 and 2 ppm K with a pure K standard solution and then compared with the reference values for the in-house MDO-G standard and the BCR-2 international geostandard. Repeated measurements of the in-house and international standards allow us to estimate uncertainties on K contents at 1%.

[24] For Ar analysis, a weighted fraction of each sample (between 0.15 and 0.28 g) was wrapped in pure Cu foil and progressively heated for 40 min up to 1500°C using a high-frequency furnace in order to allow for complete extraction of argon. Multiple-step gas cleaning was performed (using Ti foam at 700°C and SAES MP-10 getters at 400°C) in order to retain argon, the main remaining noble gas. The purified Ar was measured by mass spectrometry using the nonconventional Cassignol-Gillot K-Ar technique [*Cassignol and Gillot*, 1982]. This technique relies on a double isotopic comparison between the $^{40}Ar/^{36}Ar$ ratio of atmospheric argon and that of the sample. This direct comparison and the stable analytical conditions of the mass spectrometer require no assumption regarding the true value of the atmospheric $^{40}Ar/^{36}Ar$ ratio and there is no need for a ^{38}Ar spike in order to obtain precise measurements [*Gillot and Cornette*, 1986].

[25] Prior to each analysis, absolute calibration of the ^{40}Ar signal was performed with the measurement of a 0.1 cm^3 aliquot collected with an air pipette calibrated by volumetric determination and by repeated analyses of the inter-laboratory standard GL-O with a recommended value of $^{40}Ar^*$ of 6.679 * 10^{14} at/g [*Odin et al.*, 1982]. The typical uncertainty on the ^{40}Ar signal calibration, which is dominated by the uncertainty of the standard, is 1%. The uncertainty on the $^{40}Ar^*$ determination is a function of the radiogenic content of the sample. It is negligible in our case for old rocks containing between 58.9 and 92.4% of radiogenic ^{40}Ar (Table 1). The detection limit of mass spectrometry is 0.1% for the $^{40}Ar^*$ signal [*Quidelleur et al.*, 2001]. K/Ar ages were calculated using the ^{40}K decay constant and K abundance ratio of *Steiger and Jäger* [1977].

3.3. Results

[26] The five ^{40}K-^{40}Ar ages for the Naude's Nek section are presented in Table 1. K contents and Ar measurements were always at least duplicated for each sample and all duplicates give similar values at the 1σ level, except for NN35, which yields consistent ages at the 2σ level only (Table 1). Mean ages and uncertainties in Table 1 have been calculated by weighting each duplicate by its radiogenic ^{40}Ar content. The mean ages range from 184.8 ± 2.6 Ma to 178.3 ± 2.5 Ma considering absolute uncertainties at the 1σ level (Table 1). Whereas uncertainties on the absolute values of mean ages require that one considers the uncertainty on ^{40}Ar calibration, it is possible to calculate (smaller) uncertainties on relative ages by removing the systematic uncertainty on the standard used for the absolute calibration of the ^{40}Ar signal. This allows internal comparison of our age determinations: indeed, our samples have been collected within a single volcanic section with well-constrained stratigraphy and they have been analyzed with a single calibrated mass spectrometer. Uncertainties on relative ages are less than 1.8 Ma at the 1σ level (except for NN57-m for which it is 1.9 Ma). They are plotted on Figure 5 and are used in the following discussion. For these relative ages, only the four uppermost samples in the eruptive sequence have statistically similar ages at the 1σ level, with their means spanning 1.4 Ma (between 178.3 and 179.7 Ma) (Figure 5). These four mean ages can be averaged to yield a weighted (by $1/\sigma^2$) mean age of 179.2 ± 1.8 Ma (given a final 1% uncertainty on age determinations). On the other hand, the age obtained in the lowermost part of the eruptive sequence appears to be somewhat older and is further discussed in section 5.

4. Paleomagnetism

4.1. Previous Results

[27] The Karoo lavas have been the subject of several paleomagnetic studies over the past half century. Pioneering work was undertaken by *Graham and Hales* [1957] and *Van Zijl et al.* [1962a, 1962b]. *Van Zijl et al.* [1962a, 1962b] collected about 150 samples in two sections: Bushman's Pass and Sani Pass. Their study revealed a magnetic reversal. These earliest studies were not subject to the criteria that are now required to confidently determine primary directions of magnetization, yet the paleomagnetic pole of the Stormberg lavas (now Drakensberg Group) determined by *Van Zijl et al.* [1962b] is quite similar to that obtained more recently in Lesotho by *Kosterov and Perrin* [1996], testifying to the high quality of the early work. *Rehacek* [1995] undertook the sampling of 13 sections through the Drakensberg Group in the Lesotho remnant in order to elaborate a regional magnetostratigraphic framework. The sampling procedure consisted in collecting a few samples (3 or 4) per lava flow every three or four flows. Part of Rehacek's study was reported in a paper by *Hargraves et al.* [1997]. That paper also synthesized extensive paleomagnetic studies of the Karoo rocks (ranging from basalt and dolerites to rhyolites) by the authors, based on a total of 691 sites and 2000 samples. *Hargraves et al.* [1997] confirmed the presence of a single magnetic reversal within the Drakensberg Group, more precisely in the Mafika Lisiu unit (seven magnetostratigraphic sections are plotted in Figure 2b). Most of the sampled sections yielded statistically similar paleomagnetic directions, allowing the calculation of an overall mean pole for the Drakensberg Group. However, a pole derived from rhyolites in the upper part of the Lebombo Monocline was significantly different from the rest. The chemistry of these lavas and the presence of several magnetic reversals within the Lebombo Monocline section suggested a more complex geological history spanning a longer time period [*Jourdan et al.*, 2007a]. *Hargraves et al.* [1997] proposed that one of the magnetic reversals recorded in the Lebombo Monocline (and also found in the Sabie basalt) could be correlated with the reversal observed in the Drakensberg Group (the 1962 "van Zijl" reversal) and the Kalkrand basalt (Namibia). This magnetic correlation is also supported by geochemical similarities [*Marsh et al.*, 1997]. *Prévot et al.* [2003] have studied the magnetic reversal recorded within the Drakensberg Group in some detail. They have resampled the Bushman's Pass section in which *Van Zijl et al.* [1962a, 1962b] had found the first Jurassic magnetic reversal. Comprehensive flow-by-flow sampling allowed

Table 1. ^{40}K-^{40}Ar Ages of Naude's Nek Section Obtained in This Study[a]

Sample	Elevation (m)	K%	% ^{40}Ar*	^{40}Ar* (at/g)	Age ± 1σ (Ma)	Mean Age ± 1σ (Ma)	Polarity
NN13-m	2470	0.250	86.3	4.9841E+13	181.3 ± 2.6	179.7 ± 2.5	N
			88.2	4.9395E+13	179.8 ± 2.6		
			87.1	4.8830E+13	177.8 ± 2.5		
NN34	2152	0.244	76.2	4.6975E+13	175.6 ± 2.5	178.3 ± 2.5	N
			61.8	4.8388E+13	180.6 ± 2.6		
			81.2	4.7974E+13	179.1 ± 2.5		
NN35	2094	0.314	80.1	6.0500E+13	175.7 ± 2.5	179.7 ± 2.6	N
			86.2	6.2385E+13	180.9 ± 2.6		
			58.9	6.3340E+13	183.5 ± 2.6		
NN45	2004	0.255	88.3	5.0029E+13	178.5 ± 2.5	179.0 ± 2.5	T
			87.1	5.0333E+13	179.5 ± 2.5		
NN57-m	1900	0.404	92.4	8.2746E+13	186.3 ± 2.6	184.8 ± 2.6	R
			88.8	8.1299E+13	183.2 ± 2.6		

[a]Samples are listed in stratigraphic order from the lowest (NN57-m, 1900 m) to uppermost (NN13-m, 2470 m). K%, potassium concentration in percent; %^{40}Ar*, concentration of radiogenic ^{40}Ar in percent; ^{40}Ar* (at/g), number of atoms per gram of radiogenic ^{40}Ar; age in Ma with 1σ uncertainty; mean age in Ma (average of two or three specimens in same sample) with 1σ uncertainty; and magnetic polarity of each sample.

Prévot et al. [2003] to describe in detail the path followed by magnetic directions during the reversal. In addition to analysis of the magnetic reversal, *Kosterov and Perrin* [1996] have sampled the Mafika Lisiu and the Sani Pass sections quite extensively. They have identified magnetic directional groups within a sequence of 101 sites with normal polarity between elevations of 2350 m and 3075 m (Mafika Lisiu section) and within a sequence of 23 sites with reversed polarity between elevation 2095 m and 2390 m (Sani Pass section). This suggests brief but intense episodes of volcanic activity which are of particular interest in the context of our own study. Finally, *Kosterov and Perrin* [1996] and *Prévot et al.* [2003] reported eight magnetic directions for the Naude's Nek section: we have been able to identify in the field the holes corresponding to one of the four sites of *Prévot et al.* [2003] and to resample this flow. We compare the eight paleomagnetic directions of *Kosterov and Perrin* [1996] and *Prévot et al.* [2003] with ours below.

4.2. Laboratory Procedures and Determination of Characteristic Site Directions

[28] Paleomagnetic cores were sampled in each identified flow (section 2 and Figure 3) using a portable gasoline-powered drill. Core orientation was measured using both magnetic and sun compasses. From 8 to 10 cores, about 8–12 cm long, were collected at each paleomagnetic site, cores being distributed as widely as possible over the outcropping flow (up to tens of meters). Analyses of magnetic mineralogy and demagnetization procedures were performed at the Paleomagnetic Laboratory of Institut de Physique du Globe de Paris (IPGP; Jussieu and Saint Maur campuses). Cores were cut into 2.5 cm long specimens. Natural remanent magnetization (NRM) was measured, then stepwise-demagnetized by either alternating field (up to 100 mT with an Agico LDA-3 demagnetizer) or heating (up to 670°C in a nearly zero field laboratory-built furnace). The magnetization of samples was measured with a JR-5 spinner magnetometer in the shielded room of the Paleomagnetic Laboratory at IPGP. To detect potential changes in magnetic mineralogy during thermal demagnetization, magnetic susceptibility was monitored after each heating step using a Kappa-bridge KLY-2 instrument.

[29] Demagnetization results were plotted on both orthogonal vector endpoint diagrams [*Zijderveld*, 1967] and in equal-area projection. All data treatment and processing were performed using the Paleomac software [*Cogné*, 2003]. Magnetization components were determined by principal component analysis [*Kirschvink*, 1980] or the great circle method [*McFadden and McElhinny*, 1988].

[30] A pilot study was first undertaken in order to determine the more suitable technique for demagnetization of the entire sample collection. For each paleomagnetic site, two "sister" samples from each core were demagnetized, one by alternating field (10 steps up to 100 mT) and the other by stepwise heating (14 to 19 steps up to 670°C), respectively. Magnetic directions obtained with these two methods were compared: typical examples of demagnetization behavior are shown in Figure 6. One of the samples displayed (NN03–1) presents a well-defined characteristic remanent magnetization (ChRM), almost a single magnetization component, though the ChRM seems slightly less well determined (more "noisy") using the AF procedure. Thermal demagnetization

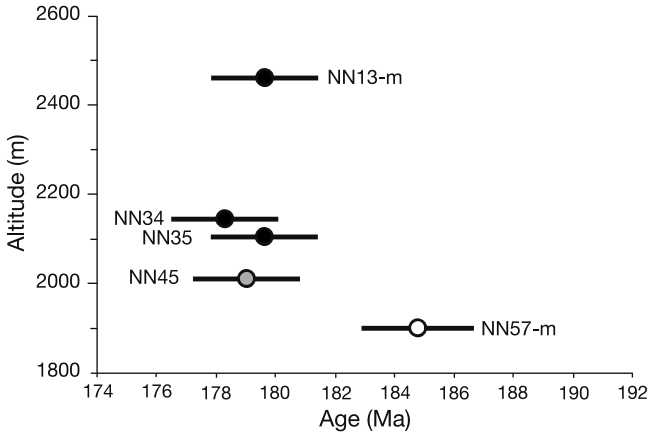

Figure 5. ^{40}K-^{40}Ar ages (see Table 1) obtained in this study, shown by circles with 1 σ total uncertainty as a function of elevation. The systematic uncertainty on the GL-O standard used for the absolute calibration of the ^{40}Ar signal is removed (see text). The magnetic polarity recorded at each dated site is shown: reverse polarity for NN57-m (open circle), transitional polarity for NN45 (gray circle), and a normal polarity for the three higher sites (black circle).

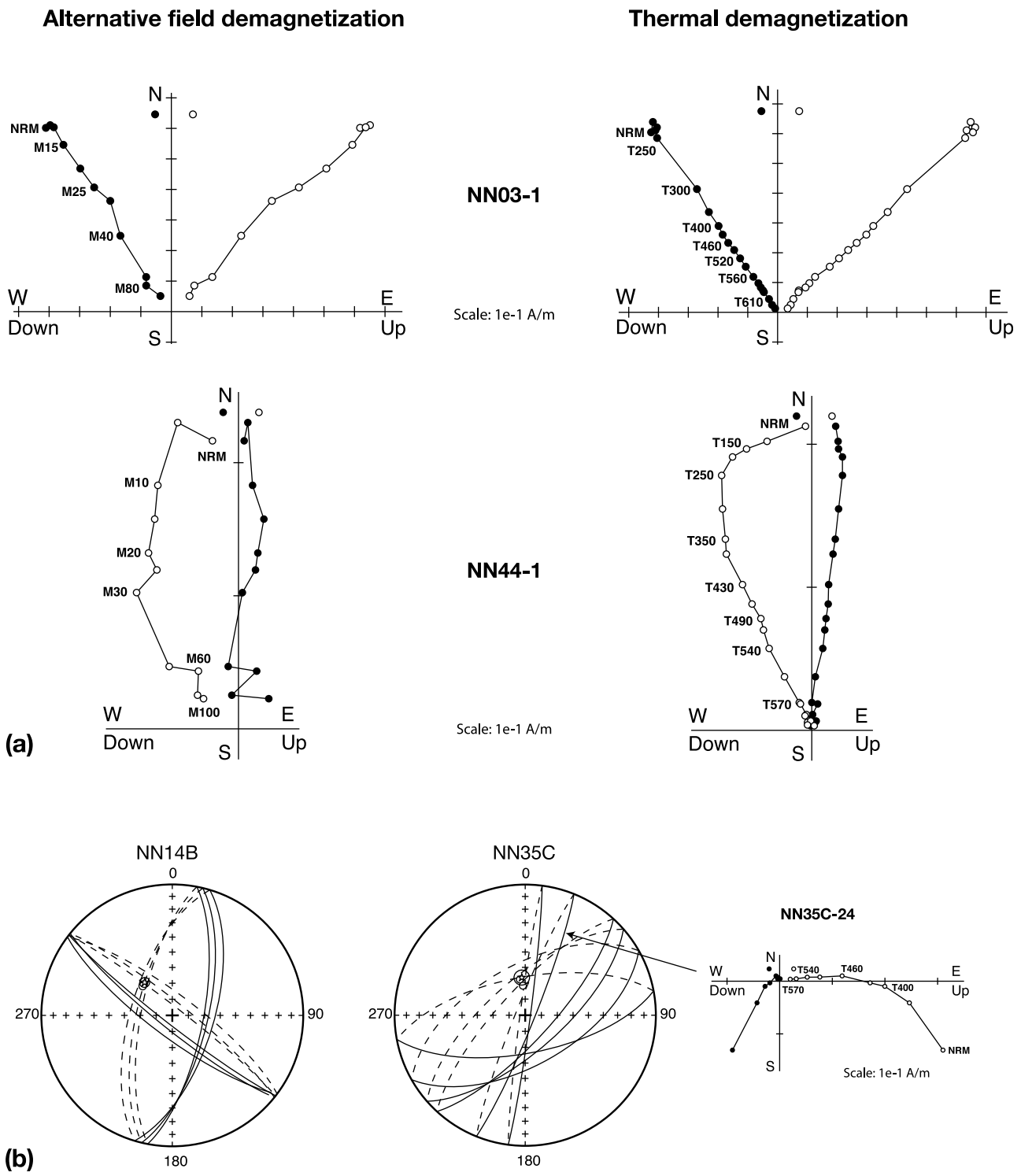

Figure 6. (a) Two examples of orthogonal projections of alternating field (M) and thermal (T) demagnetizations of pilot samples (see text). (b) Equal-area projection of great circles obtained for two sites.

of NN03–1 shows a slight change in magnetization direction after 590°C which fails to reach the origin. The characteristic component isolated between 250 and 590°C on the other hand does converge to the origin. Sample NN44–1 has a significant second, low-temperature component and displays a noisy AF demagnetization path. For most of the test samples analyzed in this way, a high-temperature component (HTC), generally directed toward the origin and associated with the characteristic primary direction, is easily determined. Complete demagnetization is generally reached between 570°C and 600°C, though some samples are fully demagnetized only at higher temperatures, up to 670°C (NN03–1). Unblocking temperatures suggest that magnetization is mainly carried by some form of magnetite (T_C = 570°C), with

Table 2. Paleomagnetic Results for the Naude's Nek Section[a]

Site	Directional Group or Single Flow	Elevation (m)	Slat (deg)	Slon (deg)	n/N	Dg (deg)	Ig (deg)	K	α_{95} (deg)	VGP Lat (deg)	VGP Lat (A) (deg)	VGP Lat (B) (deg)
NN02	DG29	2559	−30.7610	28.0890	8/8	−33.4	−42.1	275.3	3.3	59.8	75.4	70.1
NN03	DG29	2552	−30.7612	28.0882	7/8	−30.6	−38.0	99.3	6.2	61.1	74.4	67.7
NN04	DG29	2547	−30.7612	28.0873	8/8	−27.1	−45.3	161.7	4.4	66.0	80.8	73.5
NN05	DG28	2528	−30.7603	28.0862	8/8	−21.3	−55.6	261.7	3.4	71.5	88.5	81.8
NN06	DG28	2524	−30.7601	28.0860	9/9	−11.5	−60.8	67.3	6.3	75.6	79.4	78.9
NN07	DG28	2506	−30.7592	28.0850	8/8	−12.6	−56.0	64.3	7.0	78.1	82.5	77.5
NN08	DG28	2498	−30.7589	28.0843	9/9	−15.5	−57.7	423.7	2.5	75.2	84.0	80.4
NN09	DG28	2491	−30.7588	28.0839	8/8	−9.3	−58.2	192.8	4.0	78.9	79.4	76.4
NN10	DG28	2481	−30.7590	28.0831	6/8	−18.8	−52.3	2120.0	1.5	73.9	87.1	78.0
NN11	DG28	2485	−30.7597	28.0831	8/8	−16.2	−59.3	790.5	2.0	73.9	83.1	81.8
NN12	DG28	2490	−30.7603	28.0830	8/8	−17.9	−51.1	472.9	2.6	74.7	85.8	76.6
NN13	DG28	2471	−30.7601	28.0815	8/8	−15.1	−53.5	489.7	2.5	76.9	84.6	77.2
NN14B	DG27	2441	−30.7595	28.0790	8/8	−40.0	−63.1	387.1	3.1	55.9	72.7	80.1
NN15	DG27	2412	−30.7582	28.0752	8/8	−30.0	−60.4	378.3	2.9	63.7	80.6	86.7
NN16	DG27	2402	−30.7600	28.0761	9/9	−29.3	−63.7	931.0	1.7	62.9	77.8	87.1
NN17	DG27	2396	−30.7595	28.0757	8/8	−29.0	−61.0	556.7	2.3	64.3	80.6	87.7
NN18	DG27	2377	−30.7589	28.0744	8/8	−37.3	−61.0	102.4	5.5	58.3	75.7	81.9
NN19	26	2347	−30.7596	28.0736	8/8	−1.3	−55.2	162.9	4.4	84.9	73.5	69.3
NN20	DG25	2343	−30.7590	28.0730	8/8	−19.5	−54.9	97.1	5.7	73.0	88.2	80.5
NN21	DG25	2323	−30.7587	28.0714	8/8	−12.3	−54.8	195.5	4.0	78.8	82.4	76.5
NN22	DG25	2307	−30.7584	28.0703	8/8	−17.8	−52.4	239.6	3.6	74.8	86.4	77.6
NN23	DG25	2292	−30.7581	28.0694	5/8	−9.5	−54.4	2283.2	1.6	81.0	80.1	74.5
NN24	DG24	2285	−30.7580	28.0688	7/8	−24.6	−59.8	183.4	4.5	67.9	83.6	87.0
NN25	DG24	2207	−30.7615	28.0653	7/8	−25.7	−56.4	622.2	2.4	67.9	85.9	83.6
NN26B	DG24	2198	−30.7628	28.0645	6/8	−28.2	−57.3	1010.4	2.1	65.7	83.8	84.3
NN27	DG24	2211	−30.7624	28.0632	7/7	−38.9	−61.2	94.5	6.2	57.1	74.5	80.8
NN28	DG24	2206	−30.7611	28.0636	9/9	−33.1	−62.1	256.6	3.2	61.0	77.6	85.1
NN29		2202	−30.7602	28.0641	8/8	−31.1	−54.8	26.8	10.9	63.6	82.1	81.2
NN30	DG23	2194	−30.7594	28.0641	9/9	−30.2	−46.6	1694.7	1.3	63.6	80.0	74.2
NN31	DG23	2194	−30.7591	28.0641	8/8	−29.4	−48.8	161.3	4.4	64.7	81.7	76.2
NN32	DG23	2170	−30.7592	28.0627	8/8	−27.0	−49.2	117.9	5.1	66.7	83.5	76.8
NN33	22	2149	−30.7580	28.0609	7/8	−18.9	−58.2	225.4	4.0	72.6	85.3	82.8
NN34	21	2143	−30.7569	28.0620	4/8	7.4	−59.2	189.9	6.7	79.0	66.5	64.7
NN35A	20	2096	−30.7542	28.0630	6/9	−16.5	−54.3	93.0	7.0	75.6	85.9	78.6
NN35B	19	2081	−30.7558	28.0611	7/8	8.9	−51.1	66.1	7.5	82.4	64.5	60.0
NN35C	18	2057	−30.7561	28.0595	8/8	−5.2	−66.4	163.4	4.7	71.5	71.4	74.4
NN36	DG17	2060	−30.7565	28.0594	7/7	13.3	−52.1	279.3	3.6	78.6	61.1	57.4
NN37	DG17	2066	−30.7570	28.0594	8/8	12.1	−57.4	474.7	2.5	77.7	62.8	60.6
NN38	DG16	2060	−30.7576	28.0591	8/8	4.2	6.4	792.3	2.1	55.8	45.0	35.9
NN39		2051	−30.7583	28.0586	8/8	5.3	−11.6	28.4	10.8	64.6	52.0	43.3
NN40	DG16	2036	−30.7586	28.0581	8/8	4.8	4.0	423.1	2.7	56.9	45.7	36.7
NN42	DG15	2020	−30.7605	28.0577	8/8	−6.2	12.5	84.6	6.2	52.4	46.5	37.0
NN43		2015	−30.7610	28.0574	5/8	−5.5	−22.5	42.2	11.9	70.3	62.8	53.6
NN44	DG15	2007	−30.7616	28.0569	8/8	−3.8	19.8	53.2	7.8	48.8	42.1	32.6
NN45	DG15	2001	−30.7630	28.0568	8/8	−1.5	21.4	187.4	4.1	48.1	40.4	31.0
NNPR	14	2003	−30.7626	28.0554	9/9	24.1	−49.3	64.7	6.5	69.2	51.5	48.1
NN46	DG13	2001	−30.7627	28.0555	8/8	55.8	−55.4	100.6	5.5	43.7	28.7	28.9
NN47	DG13	1990	−30.7635	28.0563	7/8	60.2	−50.4	424.3	2.9	39.1	23.3	23.1
ND48		1992	−30.7641	28.0561	7/7	52.8	−58.7	23.2	12.9	46.6	32.2	32.8
ND49	12	1990	−30.7632	28.0519	8/8	39.5	−56.1	54.6	7.9	56.9	41.3	40.4
ND50		1986	−30.7633	28.0489	4/5	52.2	−50.6	48.6	13.3	45.7	29.5	28.7
ND51	DG11	1973	−30.7599	28.0444	8/8	6.8	−8.5	150.7	4.6	62.7	49.8	41.2
ND52	DG11	1967	−30.7583	28.0416	8/8	4.7	−12.8	37.7	9.7	65.3	52.9	44.2
ND53	DG11	1957	−30.7544	28.0340	8/8	−3.5	−16.7	52.0	8.3	67.5	59.0	49.9
ND54	10	1950	−30.7530	28.0336	7/8	−9.7	−44.7	54.4	8.8	80.4	76.8	68.2
ND55	DG9	1951	−30.7520	28.0334	8/8	3.5	−13.5	150.9	4.7	65.8	53.9	45.1
ND56	DG9	1946	−30.7524	28.0297	7/8	−1.2	−11.9	122.3	6.0	65.2	55.7	46.6
ND57	8	1946	−30.7523	28.0288	8/8	−2.9	−29.7	90.5	6.4	74.9	64.9	56.1
ND58	DG7	1938	−30.7513	28.0266	8/8	−0.5	−19.5	34.1	9.9	69.2	58.8	49.9
ND59		1927	−30.7536	28.0243	6/6	16.3	−23.3	44.1	11.4	66.0	49.0	41.9
ND60	DG7	1927	−30.7531	28.0208	6/6	−2.4	−18.8	295.6	4.4	68.8	59.5	50.4
ND61	DG5	1922	−30.7526	28.0195	7/7	152.1	36.0	151.9	4.9	−62.7	−74.3	−66.6
ND62	DG5	1923	−30.7515	28.0185	8/8	148.1	39.3	296.9	3.2	−60.3	−74.6	−68.4
ND63	DG5	1921	−30.7508	28.0182	4/5	144.9	34.9	145.6	7.6	−56.3	−70.5	−64.9
ND64	DG5	1906	−30.7534	28.0133	8/8	152.2	40.2	406.6	2.8	−64.1	−77.0	−69.6
ND65	DG4	1907	−30.7541	28.0130	6/8	159.6	42.5	203.9	4.9	−70.9	−79.9	−70.7
ND66	DG4	1908	−30.7546	28.0125	8/8	156.1	42.7	298.6	3.2	−68.1	−79.9	−71.4
NC07	DG3	1901	−30.7581	28.0111	8/8	166.0	50.2	208.5	3.8	−78.0	−82.6	−74.2
NC06	DG2	1900	−30.7585	28.0109	6/8	153.9	54.8	583.2	2.8	−67.8	−86.3	−82.0
NC05	DG2	1900	−30.7586	28.0106	8/8	152.6	51.1	629.0	2.2	−66.6	−84.3	−78.5
NC04	DG2	1900	−30.7589	28.0104	7/7	148.7	52.6	207.1	4.2	−63.5	−81.8	−79.2

Table 2. (continued)

Site	Directional Group or Single Flow	Elevation (m)	Slat (deg)	Slon (deg)	n/N	Dg (deg)	Ig (deg)	K	α_{95} (deg)	VGP Lat (deg)	VGP Lat (A) (deg)	VGP Lat (B) (deg)
NC03	DG2	1901	−30.7594	28.0099	8/8	153.9	56.2	267.9	3.4	−67.6	−85.8	−83.4
NC02	DG2	1898	−30.7598	28.0088	7/7	152.2	55.0	646.7	2.4	−66.4	−84.9	−82.2
NC01	DG2	1901	−30.7605	28.0060	8/8	158.9	54.8	251.2	3.5	−71.8	−89.3	−81.0
NN48	DG6	1982	−30.7816	28.0066	7/7	149.8	58.8	281.7	3.6	−63.9	−81.6	−85.3
NN49	DG6	1971	−30.7814	28.0066	4/4	154.8	62.6	201.3	6.5	−66.2	−80.3	−88.9
NN50	DG3	1957	−30.7810	28.0069	6/6	160.7	53.9	1643.5	1.7	−73.4	−88.1	−79.5
NN51	DG3	1955	−30.7810	28.0069	6/6	162.9	54.2	347.2	3.6	−75.1	−86.3	−78.8
NN52	DG3	1947	−30.7807	28.0070	5/6	162.4	51.2	199.3	5.4	−74.9	−85.7	−76.7
NN53	DG3	1942	−30.7804	28.0070	5/6	159.0	53.3	606.4	3.1	−72.0	−89.0	−79.6
NN54	DG2	1940	−30.7802	28.0069	4/5	152.4	52.9	273.2	5.9	−66.5	−84.8	−80.1
NN55	DG2	1935	−30.7802	28.0067	6/6	151.3	51.1	379.8	3.4	−65.5	−83.4	−78.3
NN56	DG2	1920	−30.7796	28.0059	6/8	152.0	53.0	284.2	4.5	−66.2	−84.6	−80.2
NN57	DG2	1909	−30.7788	28.0044	8/8	154.4	51.2	1758.3	1.3	−68.2	−85.7	−78.6
NN58	DG1	1865	−30.7813	28.0007	8/8	159.3	42.1	99.2	5.8	−70.5	−79.6	−70.5
NN59	DG1	1868	−30.7809	28.0006	4/6	157.3	43.3	377.1	4.7	−69.2	−80.5	−71.7

[a]Site mean magnetic directions (DGx when the site belongs to a directional group or x for a single flow) are numbered from 1 to 29 (see text and Table 3). Latitude Slat (deg) and longitude Slon (deg) are the coordinates of paleomagnetic sites; n/N, N is the number of samples measured, and n is the number used in calculating the mean direction; Dg and Ig are the site mean declination and inclination of the Characteristic Remanent Magnetization (ChRM); K is the Fisher precision parameter; α_{95} is the 95% confidence interval; VGP Lat is the latitude of the virtual geomagnetic pole calculated from the site mean direction; VGP Lat (A) is the VGP latitude obtained after rotation of the mean VGP (calculated after removing transitional VGPs) to the geographic pole; and VGP Lat (B) is the VGP latitude calculated using the 182 Ma South African pole of *Besse and Courtillot* [2002].

in some cases secondary hematite (T_C = 670°C), possibly with some amount of titanium involved. Lower unblocking temperature components (LTC), when they occur, are typically below 350°– 400°C (e.g., NN44–1). This secondary component is generally removed more efficiently by thermal demagnetization than by AF, and a primary ChRM can be isolated. The ChRM components we obtained using principal component analysis [*Kirschvink*, 1980] generally ranged between 460°C and 570°C. For only a few specimens the HTC could not be easily isolated from LTC. In two sites (NN14B and NN35C), many of the samples displayed significant overlap of the primary and secondary components, as shown in Figure 6b. Thus the HTC had to be determined using the great circles method, which was successful.

4.3. Site Mean Directions

[31] In light of the results of the pilot study, stepwise-thermal demagnetization was found to be the more efficient method to isolate the ChRM in most cases and it was therefore applied to the rest of the sample collection. Between six and nine cores per sites were thus thermally demagnetized (Table 2). Site-mean directions were calculated using either Fisher statistics [*Fisher*, 1953] for directions only or *McFadden and McElhinny* [1988] when both directional data and remagnetization circles had to be combined. For 76 sites, the number of samples available to calculate a site mean direction was at least 6 and up to 9. In only 10 cases was this number reduced to 4 or 5 samples, never less. Site mean directions are listed in Table 2 and illustrated as a stratigraphic log of declination, inclination and VGP latitude (Figures 7a–7c) and on an equal-area projection (Figure 8a).

[32] Only two sites (NN01 and NN41) out of 88 display inconsistent mean magnetic directions and carry a very strong (likely lightning-induced) isothermal remanent magnetization (IRM). They are consequently excluded from further analysis. The overwhelming part (85%) of site mean directions (with both polarities) have a dispersion parameter K > 100 and are therefore considered as good-quality paleomagnetic results. Dispersion in the transition zone (see below) is slightly larger, and only 40% of sites sampled in these flows have a dispersion parameter K > 100 (Table 2).

4.4. Magnetic Polarities, Transitional Directions, and Magnetostratigraphy

[33] Paleomagnetic site (flow) mean directions confirm the presence of a single reversal within the Naude's Nek section with a short sequence of reverse polarity flows at the base of the section (Table 2, Figures 7 and 8a). This is consistent with all previous studies of the Lesotho remnant [*Van Zijl et al.*, 1962a, 1962b; *Kosterov and Perrin*, 1996; *Hargraves et al.*, 1997; *Prévot et al.*, 2003]. *Kosterov and Perrin* [1996] and *Prévot et al.* [2003] report eight magnetic directions from eight lava flows, four reversed and four transitional. The approximate coordinates of the paleomagnetic sites given in the paper and the absence of any normal polarity result suggest that all samples were collected in the lower part of the section. We have been able to retrieve several of the holes left by the sampling of *Prévot et al.* [2003]. They correspond to a single flow and site, which we labeled NNPR. The magnetic direction we find for NNPR (altitude 2005 m) is transitional and is in good agreement with *Prévot et al.*'s [2003] site RH8, which is their highest altitude site (Figure 8b). Transitional directions from our sites NN47, ND51 and ND52 below NNPR match RH7, RH5 and RH4; the agreement is particularly striking for the pair NN47/RH7 (1995 m) where the mean directions are in full agreement and form the end of a distinctive loop in the reversal path, and for the pair ND51/RH5 (1975 m; Figure 8b). Several of our reversed sites below can be associated with four reversed sites from *Kosterov and Perrin* [1996], although in that case altitudes are not given by the authors and identifying corresponding samples is more difficult. We have a good to very good match of directions for RH3 with our ND63 and ND62 (1920 m), for RH2 with ND65 and ND66 (1907 m) and for both RH6 and

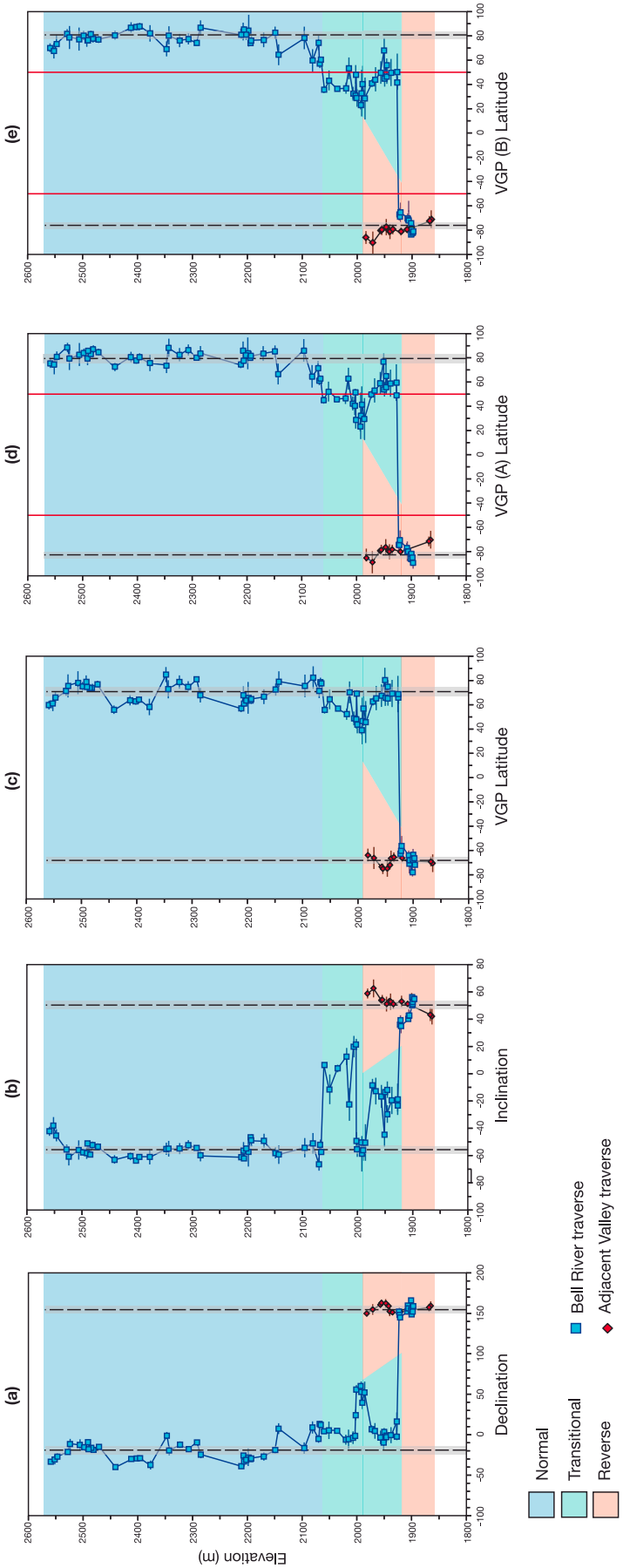

Figure 7. Magnetostratigraphic log of site mean directions of the Naude's Nek section: (a) declination, (b) inclination, (c) VGP latitudes, (d) VGP latitudes (VGP A) obtained by rotating the magnetic poles in order to place the mean VGP (calculated without transitional VGPs) at the geographic pole, and (e) VGP B latitudes calculated using the magnetic pole of the South African plate at 182 Ma from *Besse and Courtillot* [2002].

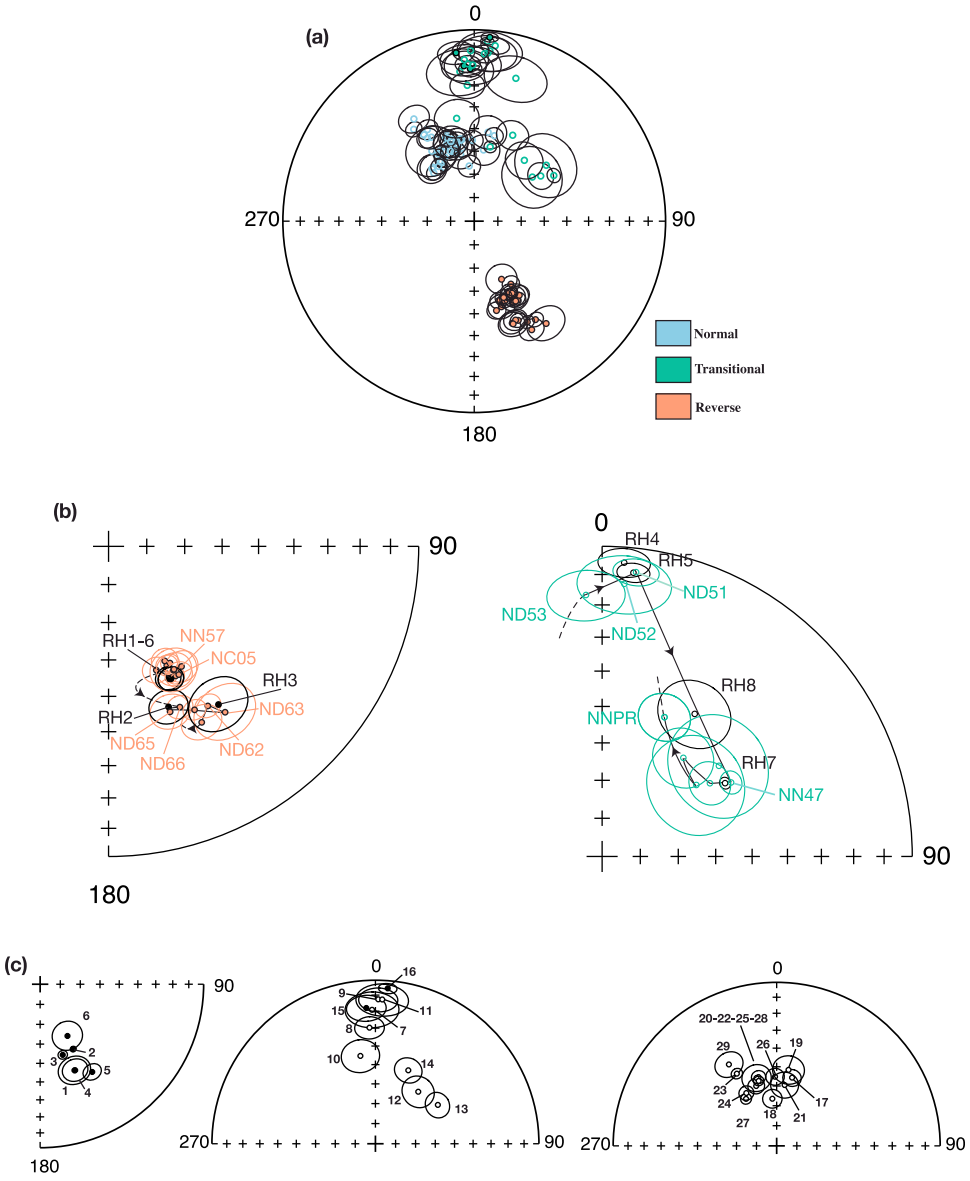

Figure 8. (a) Equal-area projection of all site mean directions and their 95% confidence intervals. Normal polarity is shown with blue circles; reverse polarity is shown with orange circles; and transitional polarity is shown with green circles. Open symbols are for upper hemisphere; solid symbols are for lower hemisphere. (b) Equal-area projection of the site mean magnetic directions obtained in this study and those obtained by previous studies of the Naude's Nek section. The left projection shows some of our reversed magnetic directions (orange) and those (four sites: RH1, RH6, RH2, and RH3, in black) obtained by *Kosterov and Perrin* [1996]. The right projection shows some of our transitional magnetic directions (in green) and those (four sites: RH4, RH5, RH7, and RH8, in black) obtained by *Prévot et al.* [2003]. (c) Equal-area projections of the 29 distinct magnetic directions (directional groups or individual lava flows) identified along the Naude's Nek section (see text and Table 3 for link between magnetic direction numbers and paleomagnetic sites). The left projection shows reversed magnetic directions; the center projection shows transitional directions; and the right projection shows normal directions.

RH1 with NN57 and NC05 (1900 m). Site NNPR is close to a rather flat area of the river and to the conspicuous Naude's Monument. All sites below were sampled in the river (over 100 m in total in terms of altitude difference), and it is understandable that the seven other *Kosterov and Perrin* [1996] sites could not be found because they might have been covered with water or eroded away since the time of sampling. However, there is little doubt that the correspondence of sites between the two studies is well established (Figure 8b).

[34] In order to determine more clearly which lava flows recorded the polarity transition, we analyzed the virtual geomagnetic poles (VGP) of each site within the section (Figure 7). Polarity is generally considered as transitional if

VGP latitude is less than 50° [*McElhinny and Merrill*, 1975]. A more elaborate scheme has been proposed by *Vandamme* [1994]. At this stage of our study, a value of 50° is used as an indicative threshold. We have first determined VGPs for all paleomagnetic sites with Africa in its present-day position (Figure 7c). We have next calculated the mean VGP, after removing (somewhat arbitrarily) transitional VGPs. Magnetic poles have then been rotated in order to place the mean VGP at the geographic pole, and the corresponding VGP latitudes (VGP A) are plotted in Figure 7d. Lava flows displaying VGP latitudes between −50° and 50° are then considered as transitional. We also determined the position of VGPs with Africa in its Early Jurassic position, using *Besse and Courtillot*'s [2002] reconstructions and synthetic apparent polar wander paths (APWP). Again, we use a latitude threshold of 50° to define which lava flows have recorded a transitional polarity (VGP B in Figure 7e). The two methods yield similar results. Twenty-three lava flows sampled in the BR traverse between 1927 m and 2060 m (~135 m thickness) have recorded a transitional polarity. The lower 25 sites (~130 m thick, elevation <1927 m) of the section have recorded a reversed polarity, whereas the upper 38 sites (~520 m thick, elevation >2060 m) have normal polarity. All lava flows collected in the AV traverse display a reversed polarity, despite an elevation which is well above that of the first transitional lava flow in BR, an important observation which is explained below.

4.5. Directional Groups

[35] *Mankinen et al.* [1985] observed that a set of successive lava flows in the Steens Mountain (part of the ~15 Ma old Columbia River flood basalts in the Western U.S.) displayed similar magnetic directions, that is, strong overlap of their small 95% confidence cones. These directions could therefore be averaged with statistical significance, and the resulting magnetic direction was termed a "directional group" (DG). The significance of such DGs is that they represent (often very large) volumes of lava that were erupted too fast for secular variation to be recorded. Such directional groups have now been observed within volcanic sequences in several large igneous provinces: the Central Atlantic Magmatic Province [*Knight et al.*, 2004], the North Atlantic igneous province [*Riisager et al.*, 2002, 2003], the Deccan traps [*Chenet et al.*, 2008, 2009], the Siberian traps [*Pavlov et al.*, 2010], and the Columbia River basalts [*Jarboe et al.*, 2008].

[36] Study of the behavior of the Earth's magnetic field on historical timescales shows that the correlation time of nondipole features does not exceed about 300 years [*Hulot and Le Mouël*, 1994]. Using an extensive archeomagnetic database, *Gallet et al.* [2002] have shown that the geomagnetic field direction in Europe has varied by as much as ~10° in inclination and ~15° in declination over the past 400 years, and as much as ~18° in inclination and ~50° in declination over the past 3000 years [*Gallet et al.*, 2003]. *Chenet et al.* [2008] have calculated the distribution of along-track secular variation velocities for the same time period. The distribution displays a lognormal shape with a strong mode at about 2° per century and a median at about 3° per century. Assuming that this value remains valid on geological timescales, *Chenet et al.* [2008, 2009] concluded that emplacement of successive lava flows displaying magnetic directions differing by no more than a few degrees, about 3°, had been emplaced over no more than ~100 years. DGs can therefore be used as a relative chronometer, in the sense that they allow one to identify flow fields that erupted in a very short time. Of course, one can (unfortunately) not estimate in this way the amount of time between flows with significantly different directions, which can be either quite short or very long.

[37] Note that finding that DGs are associated to sometimes huge lava ensembles that may have cooled in decades only or even less is fully consistent with the estimate of time required to erupt the Roza flow (about 1600 km^3) in the Columbia River basalt based on physical volcanology and fluid dynamics [e.g., *Thordarson and Self*, 1998]: this did not exceed a few years.

[38] Various criteria have been used to define directional groups. We use here the criteria defined by *Chenet et al.* [2008, 2009], which consist in assuming that a set of superimposed lava flows with similar paleomagnetic directions define a directional group. To test quantitatively the validity of this assumption, the distances between the mean magnetic directions of the directional group on one hand, and each site-mean direction on the other hand, must be lower than a threshold value defined as the root square of the sum of the squares of the 95% confidence cones of the directional group and the paleomagnetic sites. This criterion must be fulfilled by each paleomagnetic site within a directional group. Six paleomagnetic sites (NN29, NN39, NN43, ND48, ND50 and ND59) which had a large α_{95} (>10°) were excluded from that analysis (Table 2).

[39] This left 80 paleomagnetic sites, from which 29 distinct magnetic directions could be defined (Table 3 and Figure 8c): 19 directional groups were found, and only 10 lava flows yielded individual magnetic directions that could not be merged with either underlying or overlying flows. The site mean directions for all paleomagnetic sites are plotted in Figure 8a, whereas the mean magnetic directions of DGs and single lava flows are represented in Figure 8c.

[40] The ~500 m thick upper part of the section has recorded a normal polarity (Figures 7 and 9). Within this part of the section, seven directional groups and six distinct magnetic directions have been defined. The number of lava flows originally identified in the field and the log (Figure 3) within each DG varies between two and nine, and DG thicknesses vary between 15 m and 100 m. The thickest are DG24 (~80 m and five sampled lava flows), DG27 (~100 m and five sampled lava flows) and DG28 (~60 m and nine sampled lava flows). The seven DGs represent 66% of the total thickness of the volcanic pile. Three successive paleomagnetic sites, NN35A, NN35B and NN35C, that had been sampled in what appeared in the field as a single cooling unit, actually display magnetic directions which are distinct from each other. Although we had found no clear evidence of lava flow limits in the field, our paleomagnetic technique in this case "works in the opposite sense" by indicating a more complex structure with thinner cooling units rather than a bunching of flows into a thicker one.

[41] Within the ~135 m thick intermediate part of the Naude's Nek section which has recorded a reversal, six directional groups and four individual magnetic directions are identified. Three paleomagnetic sites exhibiting large α_{95} are excluded from the calculation (larger α_{95} are expected in

Table 3. Distinct Magnetic Directions Numbered From 1 to 29 in Stratigraphic Order[a]

Directional Group or Single Flow	Site(s)	N	Dg (deg)	Ig (deg)	K	α_{95} (deg)
DG29	NN02 to NN04	3	329.6	−41.8	347.1	6.6
DG28	NN05 to NN13	9	344.5	−56.1	435.0	2.5
DG27	NN14B to NN18	5	326.9	−61.9	821.8	2.7
26	NN19	1	358.7	−55.2	162.9	4.4
DG25	NN20 to NN23	4	345.2	−54.2	738.6	3.4
DG24	NN24 to NN28	5	330.1	−59.5	445.4	3.6
DG23	NN30 to NN32	3	331.1	−48.2	2077.4	2.7
22	NN33	1	341.1	−58.2	225.4	4.0
21	NN34	1	7.4	−59.2	189.9	6.7
20	NN35A	1	343.5	−54.3	93.0	7.0
19	NN35B	1	8.9	−51.1	66.1	7.5
18	NN35C	1	354.8	−66.4	163.4	4.7
DG17	NN36, NN37	2	12.7	−54.8	465.4	σ = 4.4
DG16	NN38,NN40	2	4.5	5.2	2184.5	σ = 3.4
DG15	NN42, NN44, NN45	3	356.1	17.9	239.4	8.0
14	NNPR	1	24.1	−49.3	64.7	6.5
DG13	NN46, NN47	2	58.1	−52.9	403.8	σ = 6.2
12	ND49	1	39.5	−56.1	54.6	7.9
DG11	ND51 to ND53	3	2.7	−12.7	146.7	10.2
10	ND54	1	350.3	−44.7	54.4	8.8
DG9	ND55, ND56	2	1.1	−12.7	557.4	σ = 7.6
8	ND57	1	357.1	−29.7	90.5	6.4
DG7	ND58, ND60	2	358.5	−19.2	3818.2	σ = 10.8
DG6	NN48, NN49	2	152.1	60.7	641.7	σ = 7.4
DG5	ND61 to ND64	4	149.3	37.6	461.5	4.3
DG4	ND65, ND66	2	157.8	42.6	1965.5	σ = 5.9
DG3	NN50 to NN53; NC07	5	162.3	52.6	1165.7	2.2
	NC07	1	166.0	50.2	208.5	3.8
dg3a	NN50 to NN53	4	161.3	53.2	2275.4	1.9
DG2	NN54 to NN57; NC01 to NC06	10	153.0	53.3	1135.4	1.4
dg2b	NC01 to NC06	6	153.3	54.1	913.6	2.2
dg2a	NN54 to NN57	4	152.5	52.1	3744.9	1.5
DG1	NN58, NN59	2	158.3	42.7	3701.9	σ = 7.5

[a]DGx is for a directional group, and X only is for a single flow. See text. N represents the number of paleomagnetic sites defining the cooling unit (1 for a single flow; from 2 to 10 for directional groups). In the case when N = 2, α_{95} cannot be calculated and the value $\sigma = \sqrt{(\alpha_{95-1}^2 + \alpha_{95-2}^2)}$ is listed. Other column headings are the same as those in Table 2.

lower transitional field intensities). The number of lava flows within a DG varies from two to four. In term of thickness, the DGs still represent about two thirds of this part of the section; however, the mean thickness does not exceed 30 m (DG15). Both the thickness of DGs and the number of lava flows within a DG are therefore significantly smaller than those in the upper, normally magnetized part of section. This would be consistent with an increase of secular variation recorded during the reversal.

[42] The lower part of the section was reconstructed from geographically composite locations (Figures 3 and 9), and we first analyze the Bell River (BR) traverse (~30 m thick) and the adjacent small valley (AV) traverse (~110 m thick) separately. In the BR traverse, three directional groups and one distinct magnetic direction (flow NC07) are identified. In the AV traverse, we isolate four directional groups. Directional groups identified along a profile, which can then be correlated with another DG or lava flow from the other profile, are labeled *dgxa* for the AV traverse and *dgxb* for the BR traverse. At the bottom of this section, DG1 is defined by flows NN58 and NN59 (NN58 belongs to an unknown geochemical unit; see section 2). Then *dg2a* (33 m thick at least) is defined by four flows (from NN54 to NN57), *dg3a* by four flows (from NN50 to NN53) and finally DG6 by two flows (NN48 and NN49). *dg2a*, *dg3a* and DG6 belong to the Moshesh's Ford unit.

[43] Within the BR traverse, we identify three directional groups *dg2b*, DG4 and DG5 and an individual lava flow (NC07). These three DGs and the single lava flow have recorded a reversed polarity. Two lower DGs (*dg2b* and DG4) and the single lava NC07 belong to the Moshesh's Ford unit whereas DG5 belongs to the Mafika Lisiu unit. A comparison of the DGs and individual magnetic directions between the BR and AV traverses allows us to correlate them and construct a single, consistent log of the Naude's Nek volcanic sequence (Figure 3). DG1 cannot be linked to any single lava flow or cooling unit from the BR traverse. *dg2a* in the AV traverse displays the same magnetic direction as *dg2b* in the BR traverse; both taken together define a well-determined directional group DG2. The thickness of *dg2b*, comprising flows NC01 to NC06, does not exceed 10 m, much less than the 33m of *dg2a*. However, we have not been able to collect cores between NN58 (DG1) and NN57 (*dg2a*) because of the absence of reachable outcrops in the AV traverse and below NC01 in the BR traverse. The next directional pulse *dg3a* in the AV traverse and the individual site NC07 in the BR traverse display a statistically similar magnetic direction, which allows us to define a cooling unit DG3. The respective thicknesses of *dg3a* and NC07 are different, which can be owing to flow geometry. The next DGs in the AV traverse (DG6) and in the BR traverse (DG4) have recorded two distinct magnetic

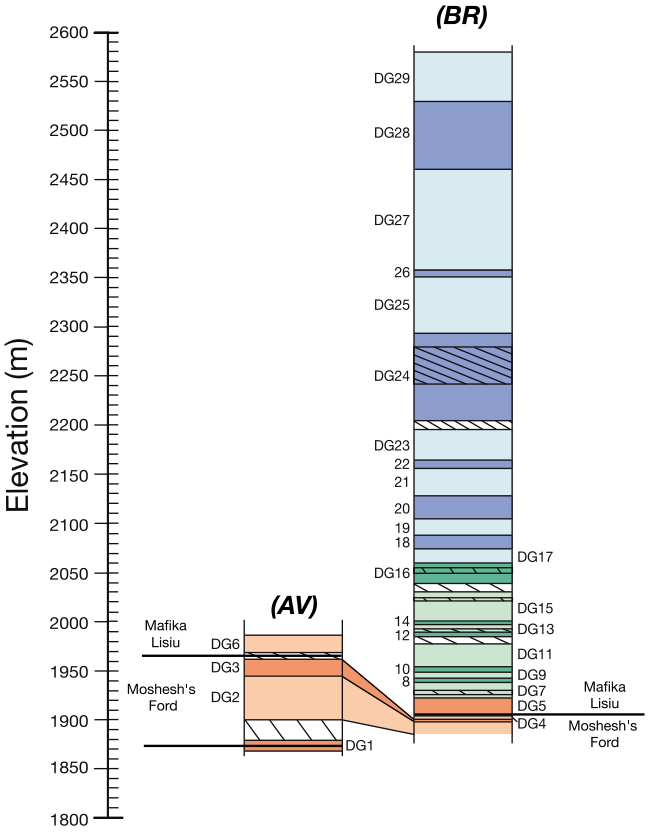

Figure 9. Stratigraphic log of the 29 distinct magnetic directions (directional groups or individual lava flows) for the Naude's Nek section as a function of elevation (color scale as in Figure 8a). Magnetic correlations between the BR and AV traverses are shown. The geochemical limit between the Moshesh's Ford and Mafika Lisiu units is also represented. The stratigraphic location of this limit within the BR section is based on geochemical analyses (J. Marsh, unpublished data, 2010); within the AV traverse, it is estimated according to paleomagnetic correlations between the AV and BR traverses.

directions. The cooling unit DG4 is the last cooling unit belonging to the Moshesh's Ford unit within the BR traverse. The first DG belonging to the Mafika Lisiu unit is DG5. Considering flow geometry, directional group DG6 identified in the AV traverse may represent the first cooling unit of the Mafika Lisiu unit.

[44] The above correlations allow us to unambiguously connect the BR and AV sections. The correlation is illustrated in Figure 10. The section in Figure 10 follows the dashed broken line shown in Figure 4, in order to take into account the major change in azimuth of the sampled sections. Sampling of the Naude's Nek section was actually performed in two successive years, and in the first year, we had stopped sampling of the BR river section at site ND54, that is, at 1950 m altitude and had resumed sampling at a higher altitude (site NN48 at 1982 m) on the AV section. Yet we could not find any paleomagnetic evidence of overlap between the two: this was simply due to the slight slope of the flows and the long distance between sites as was resolved by further sampling downstream of BR in the second field season. The correlation of magnetic directions between the AV and BR traverses suggests that the whole section is tilted by about 1° toward the north or northeast. The implication of our interpretation is that, whereas flows appear to be flat-lying on an E-W cross section, they are actually sloping by about 1° to the north when seen on an almost N-S section (Figure 9). This is presumably due to lava emplacement over a slightly tilted paleosurface of the Clarens formation. The boundary between the Moshesh's Ford and Mafika Lisiu units is located between *dg3a* and DG6 (note that our numbering scheme respects stratigraphic order with DG3, 4, 5 and 6 in that order from older to younger).

4.6. Reversal Test and Magnetic Poles

[45] The presence of both normal and reversed polarity directions allows a reversal test to be performed [*McFadden and Lowes*, 1981; *McFadden and McElhinny*, 1990]. The mean magnetic direction for normal polarity sites is D = 340.8°, I = −56.2° (α_{95} = 2.8°, k = 69, N = 38) and for reversed polarity sites D = 334.9°, I = −49.6° (α_{95} = 2.9°, k = 103.2, N = 25). Although the two directions are only 5.9° apart, their 95% confidence intervals are so small that the reversal test fails. In order to check whether overrepresentation of some magnetic directions (comprising DGs) might have led to failure of the reversal test, we have calculated mean directions not on the basis of all site means but by combining only those obtained for DGs and individual lava flows not involved in DGs. The corresponding mean magnetic directions are D = 346.9°, I = −56.4° (α_{95} = 5.6°, k = 55, N = 13) for normal polarity and D = 335.5°, I = −48.3° (α_{95} = 7.7°, k = 77.4, N = 6) for reversed polarity. However, the reversal test fails again, though confidence intervals now intersect.

[46] A first cause for failure of the test might be due to the small number of determinations (only six in the latter case for reversed polarity) and lack of proper averaging of paleosecular variation. After converting the mean magnetic directions to VGPs, we find that the angular standard deviations (ASD) for the four means calculated above range between 7.7 and 14.2°. The ASD for reversed polarity is 7.7° using paleomagnetic sites and 8.7° using DGs and individual lava flows. The ASD for normal polarity is significantly larger, with corresponding values of 12.5° and 14.2°. These are about half of those proposed by *McFadden et al.* [1991] for the paleolatitude of Karoo in the period range between 110 and 195 Ma. Our data, in particular those with reversed polarity, might have failed to average secular variation. Another cause might be the presence of a remaining, unremoved secondary overprint. Indeed, the declinations being close to 360°/0°, the difference in inclinations is compatible with a small remaining normal overprint that would have failed to be removed by thermal demagnetization and would have an unblocking temperature spectrum similar to that of the primary component. An overprint of about 10% of the NRM would be sufficient. A similar situation was encountered in the Deccan traps by *Vandamme et al.* [1991]. In any case, there can hardly be doubt that a genuine reversal has indeed been recorded by the Karoo-Lesotho lavas, and that the whole set of characteristic directions we have determined for the Naude's Nek section does represent the paleofield accurately.

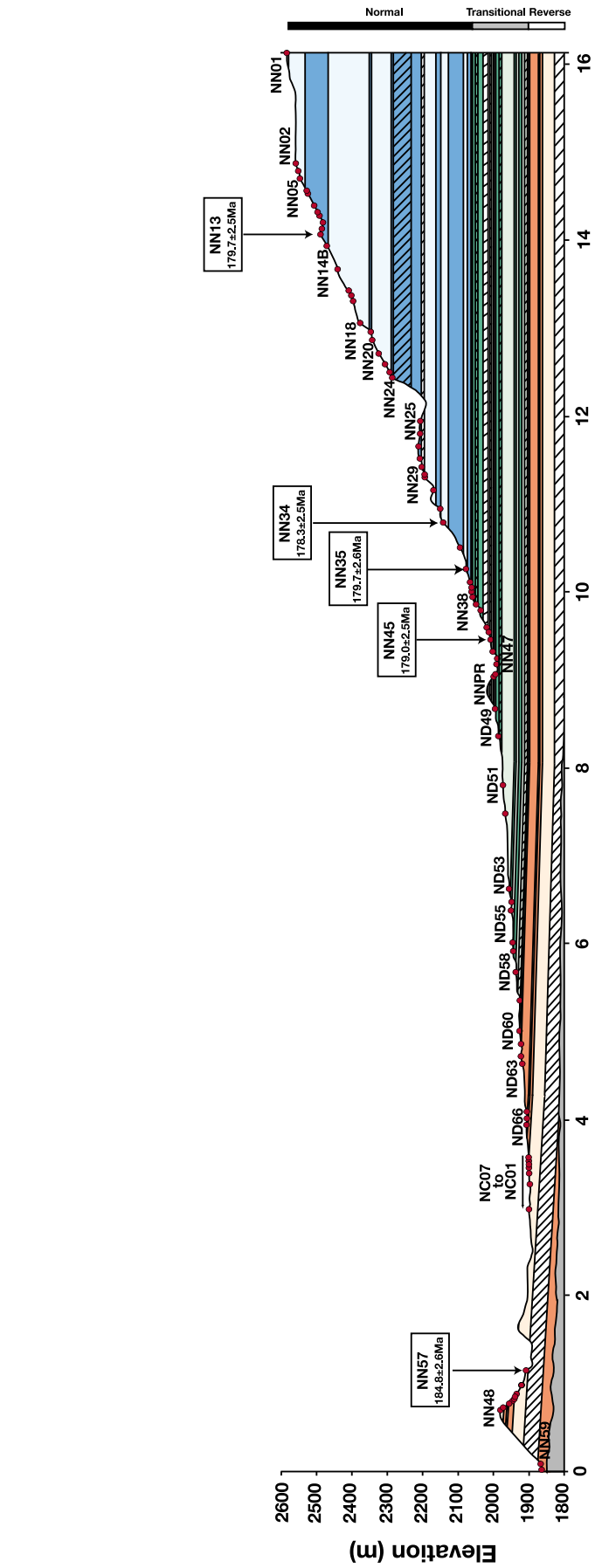

Figure 10. Cross section of the Naude's Nek eruptive sequence (the cross section is drawn along the dashed line displayed in Figure 4) with the 86 paleomagnetic sites (small red circles) and the five dated sites (boxes, ages with 1 σ total uncertainties). Magnetic polarity and directions (i.e., separate directional groups or individual lava flows; color scale is the same as that in Figure 8d) are shown (and extrapolated laterally). The hatched levels could not be sampled.

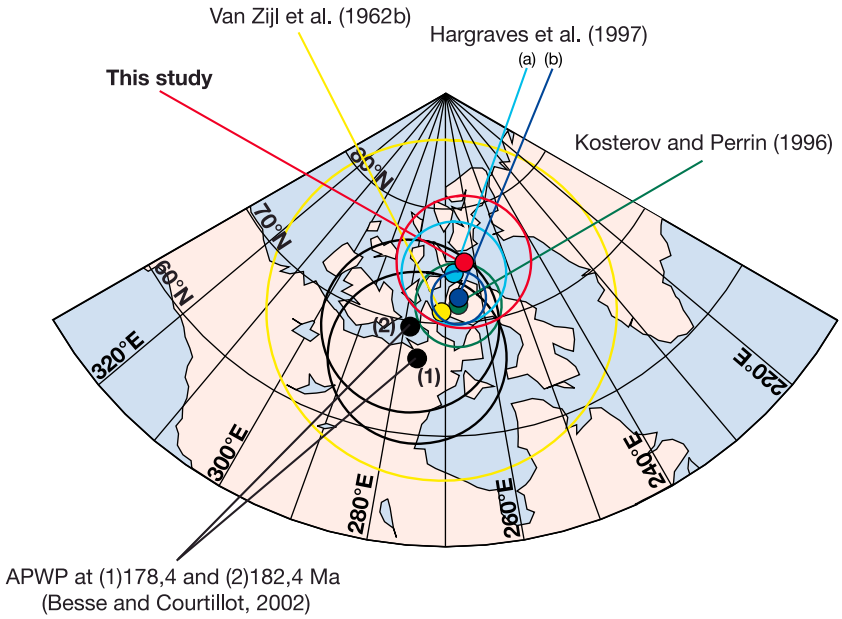

Figure 11. Equal-area projection of virtual geomagnetic poles for the Drakensberg Group with 95% confidence intervals projected on the Northern Hemisphere. The red circle shows our mean VGP; the yellow circle shows that from *Van Zijl et al.* [1962b]; and the green circle shows that from *Kosterov and Perrin* [1996]. The blue circle (labeled "a") corresponds to the mean VGP of *Hargraves et al.* [1997] calculated with the 11 mean magnetic poles for each of the sampled sections within the Lesotho remnant (data in Appendix 1 of *Hargraves et al.* [1997]). Pole KAT from *Hargraves et al.* [1997] presents a large 95% confidence interval (18.5°) and hence is excluded from the recalculated VGP for the Drakensberg Group (dark blue circle, labeled "b"). Black circles correspond to the synthetic reference poles of *Besse and Courtillot* [2002] for South Africa at 182.4 Ma and 178.4 Ma.

[47] We next calculate an overall mean paleomagnetic direction for the Naude's Nek section using the mean magnetic directions of all DGs and individual lava flows, excluding transitional directions (Table 3). We obtain an overall mean direction D = 342.8°, I = −54.0° (α_{95} = 4.7°, k = 51.0, N = 19). The coordinates of the overall mean virtual geomagnetic pole (VGP) deduced from this overall mean direction are λ = 75.2°N, φ = 276.4°E (A_{95} = 5.8°, K = 34.8, N = 19).

[48] The first paleomagnetic pole determined by *Van Zijl et al.* [1962b] was based on 132 cores and 74 paleomagnetic sites sampled along the 1300 m thick section at Sani Pass and along a 1000 m thick section in the Maseru area (Figure 2): coordinates were λ = 71°N, φ = 269°E (A_{95} = 15°, N = 74). More than 3 decades later, *Kosterov and Perrin* [1996] calculated a better resolved magnetic pole for the Drakensberg Group with coordinates λ = 71.6°N, φ = 273.5°E (A_{95} = 3.7°, K = 33, N = 47): though the confidence interval had decreased by a factor 4, the means were separated by less than 2°. *Hargraves et al.* [1997] published thirteen paleomagnetic poles corresponding to different volcanic remnants (lava flows, dykes and sills). They calculated a pole on the basis of mean VGPs of 11 sections distributed throughout the Lesotho remnant. Although this pole is within the 95% confidence interval of the two paleomagnetic poles determined by *Van Zijl et al.* [1962b] and *Kosterov and Perrin* [1996], it is still slightly more distant. One of the VGPs corresponding to the Katse Dam section (KAT) seems doubtful (given its large A_{95} = 18.5°). We have recalculated a mean pole excluding the Katse Dam result: it is located at λ = 72.3°N, φ = 273.5°E (A_{95} = 2.3°, K = 427.4, N = 10), very close to the poles obtained by *Van Zijl et al.* [1962b] and *Kosterov and Perrin* [1996].

[49] These poles and that from the present study are plotted in Figure 11. The poles from *Van Zijl et al.* [1962a, 1962b], *Kosterov and Perrin* [1996], and *Hargraves et al.* [1997] are all within our 95% confidence interval, which (because we are working here with a single magnetostratigraphic section) is still rather large at 5.8°. We believe that our pole can still be considered valid and entered into the global database, despite failure of the reversal test.

[50] We next compare these poles with the synthetic reference poles of *Besse and Courtillot* [2002] for South Africa. Our pole is statistically indistinguishable at the 95% confidence level from the reference pole of *Besse and Courtillot* [2002] at 182.4 Ma. The 178.4 Ma pole is only marginally farther away.

5. Discussion and Conclusion

[51] We first compare our new age determinations with those previously reported and obtain some constraints on the number of phases and on the total duration of Karoo volcanism in the Naude's Nek section and, more generally, in Lesotho. We next use the new paleomagnetic results to provide higher resolution, but relative and discontinuous, constraints on the existence of larger magmatic pulses.

[52] The five samples we dated with reasonable accuracy within the Naude's Nek section yielded K-Ar ages, only one

of which could be statistically distinguished from the others (Figure 5). Sample NN57-m collected from the lowermost flow of the Naude's Nek section (Figure 3; 1909 m asl) appears to be somewhat older than the four other samples at the 1σ level (after removing uncertainties used to calculate ages, see section 3). The age of the lowermost flow (which may belong to the Moshesh's Ford unit) is 184.8 ± 2.6 Ma and the age of the average of the rest of the lava pile above (collected within the Mafika Lisiu unit at NN45, NN35, NN34 and NN13-m) is 179.2 ± 1.8 Ma (Figure 12). The K-Ar dating technique does not allow one to evaluate radiogenic ^{40}Ar loss and one can never rule out the hypothesis such loss occurred, which would lead to slightly younger ages. However, we consider that such a phenomenon is not significant here on the basis of the consistency of the four uppermost ages from the section (all statistically identical at the 1σ level). This could be an indication that volcanism in the Naude's Nek area occurred in two successive phases, separated by a few million years, with the lower one being far less voluminous than the upper.

[53] We next compare the new K/Ar age determinations with previously reported ages from the Lesotho remnant. *Jourdan et al.* [2007b] have dated five plagioclase separates (using the laser stepwise-heating ^{40}Ar/^{39}Ar technique) from samples collected in the northern part of the Lesotho magmatic province: two from the Maseru area (ROM-01 and BUS-18), one from the Oxbow section (OXB-01) and two from the Sani Pass section (SA77; SA79) (Figures 2b and 12). These five samples encompass almost the entire lava sequence in northern Lesotho: the three samples ROM-01 (1950 m asl, first flow above the Clarens Sandstone Formation), SA79 (2129 m) and SA77 (2090 m) belong to the Golden Gate geochemical unit, BUS-18 (2239 m) belongs to the Mafika Lisiu unit and OXB-01 (3305 m, at the very top of the Oxbow section) belongs to the Mothae unit (Figure 2b). The five ^{40}Ar/^{39}Ar plateau ages are statistically indistinguishable at the 1σ level. The overall weighted mean is 181.6 ± 0.4 Ma (at 1σ) [*Jourdan et al.*, 2007b]. Clearly, the small uncertainty (0.2% at 1σ) associated with this weighted mean cannot have included the uncertainty of the J determination nor the one associated with the standard's age (see below). These ages were calculated using a J value determined with the age of the Hb3gr hornblende standard at 1072 Ma [*Turner et al.*, 1971]. This age is equivalent to the astronomically tuned age of 28.02 Ma generally used for the Fish Canyon sanidine standard, which is itself compatible with an age of 523.1 Ma for the MMhb-1 standard [*Renne et al.*, 1994, 1998]. The MMhb-1 standard has been dated at 525 ± 2 Ma [*Fiet et al.*, 2006] using the same instrument and analytical conditions as used in the present study. This age is thus compatible with that proposed by *Renne et al.* [1998] and the new K/Ar ages are directly comparable with those proposed by *Jourdan et al.* [2007b].

[54] Over a decade ago, *Duncan et al.* [1997] reported a ^{40}Ar/^{39}Ar age of 183.9 ± 0.7 Ma for a plagioclase separate (KF-10) from a sample belonging to the Omega geochemical unit collected in the Kraai River Pass section (Figure 2b). This age was calculated using the Fish Canyon biotite standard dated at 28.03 Ma. This age has been recalculated by *Jourdan et al.* [2007b], using the Fish Canyon sanidine-biotite intercalibration factor of 1.005 ± 0.17 proposed by *Dazé et al.* [2003], leading to an age of 184.7 ± 1.0 Ma for the Kraai River Pass section. This older age was subsequently thought to be incompatible with the ages obtained by *Jourdan et al.* [2007b], and the discrepancy was attributed to excess ^{40}Ar* and/or standard heterogeneity. ^{40}Ar/^{39}Ar ages are relative to standards used as neutron flux monitors, they are not absolute ages in themselves. The ages of these standards have been episodically revised by more than 1% over the past two decades and will likely be revised again in the future. As an example, the age of the widely used Fish Canyon Tuff sanidine (FC-san) standard is subject to controversy, with proposed values ranging from 27.5 Ma to 28.2 Ma, a difference of more than 2% [*Renne et al.*, 1994, 1998; *Lanphere and Baadsgaard*, 2001; *Spell and McDougall*, 2003; *Kuiper et al.*, 2004]. Recently the age of FC-san has been further revised twice, first at 28.201 ± 0.023 Ma (1σ) using an astronomical calibration [*Kuiper et al.*, 2008], then (based on reinvestigation of the ^{40}K decay constants and ^{40}K/^{40}Ar* content of FC-san) at 28.305 ± 0.036 Ma (1σ) [*Renne et al.*, 2010]. Note that, given their very small uncertainty, these ages are consistent only at the 2σ level. However, because the issue regarding the true age of FC-san still appears unresolved, we prefer to conservatively use the age of 28.02 Ma [*Renne et al.*, 1998]. Furthermore, in order to account for potential uncertainties not fully accounted for by standard ages, we allow for a minimum uncertainty of 1% on all published ages. This yields a recalculated weighted mean of 181.6 ± 1.8 Ma for the mean age of the five samples from *Jourdan et al.* [2007b] and 184.7 ± 1.8 Ma for the Kraai River Pass sample of *Duncan et al.* [1997].

[55] We see from the synthesis in Figure 12 that the hypothesis that Karoo volcanism in Lesotho could have occurred in two distinct phases is supported, although statistically only marginally, by the earlier results of *Jourdan et al.* [2007b] and *Duncan et al.* [1997]: their two mean ages agree with those we find in the Naude's Nek section. The first (smaller) eruptive phase would correspond to the emplacement of the lower part of the volcanic pile (entirely of reversed polarity) in the southern part of the Lesotho remnant at ~185 Ma. The second, separate eruptive event would have taken place 3 to 5 Myr later and correspond to the emplacement of the upper part of the volcanic pile (starting with reversed DG6, then encompassing the reversal and the normal polarity sequence), covering the entire Lesotho remnant. Since the age obtained for the top of the basalt sequence in the Oxbow section by *Jourdan et al.* [2007b] is statistically similar to the lowermost ones in Sani Pass and to our own ages in the Naude's Nek section down to sample NN45 (in the transitional polarity zone), we suggest that the entire volcanic pile situated above NN45 (NN45 included, i.e., about 500 m thick) was emplaced over a period of time not exceeding 2 Myr (upper limit given the uncertainties), in agreement with the shorter 0.8 Myr duration estimated by *Jourdan et al.* [2007b]. Because sample NN45 has recorded a transitional magnetic direction and because the duration of a reversal is only a few kyr (i.e., almost instantaneous with respect to the estimated duration of the eruptive phase), we suggest that the lava flows which have recorded transitional polarities were all emplaced

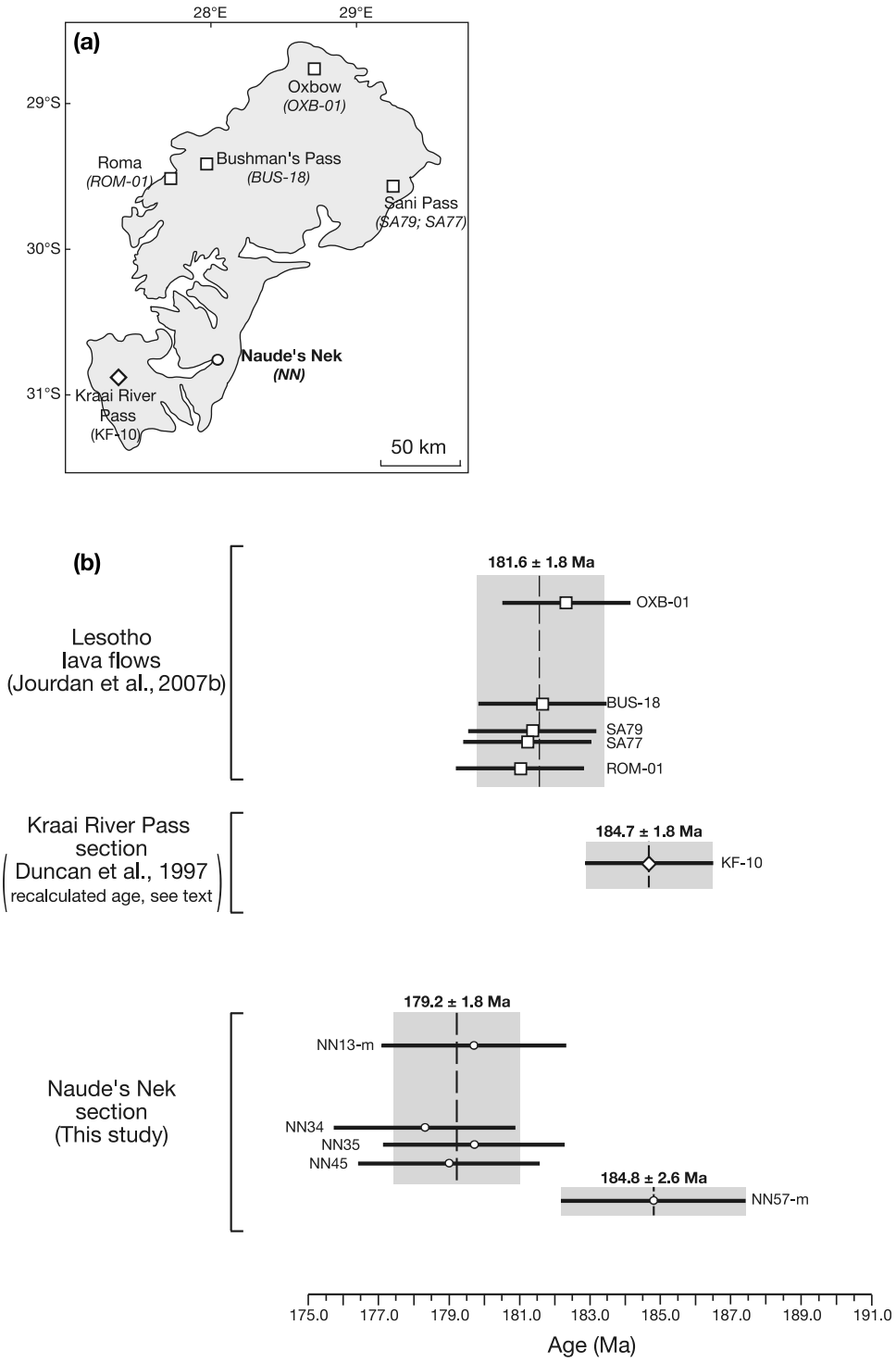

Figure 12. (a) Location of sites with age determinations within the Lesotho volcanic province (shown in gray). Sample KF-10 is from *Duncan et al.* [1997]; samples OXB01, ROM-01, BUS-18, SA77, and SA79 are from *Jourdan et al.* [2007b]; and NN is this study. (b) Comparisons of the ^{40}K-^{40}Ar (this study) and published $^{40}Ar/^{39}Ar$ ages: the data in each subset are plotted in stratigraphic order. The dashed lines and shaded gray bands represent the mean age and uncertainties for each subset, respectively. The $^{40}Ar/^{39}Ar$ age (KF-10) of the Kraai River Pass section obtained by *Duncan et al.* [1997] has been recalculated by *Jourdan et al.* [2007b] using the Fish Canyon sanidine-biotite intercalibration factor of 1.005 ± 0.17 proposed by *Dazé et al.* [2003]. In order to account for the potential uncertainties on ages of standards, we assume a minimum uncertainty of 1% (at the 1σ level) on all absolute and mean ages. Geological timescale is after *Ogg et al.* [2008]: age of the Pliensbachian-Toarcian boundary, 183 ± 1.5 Ma.

during the second eruptive phase. These results imply that all flows including and above NN49 (Figure 3), comprising the entire 650m thick Mafika Lisiu unit, were emplaced during the second eruptive phase, over a time span on the order of 1 Myr and possibly much less.

[56] The older age of the sample collected within the Moshesh's Ford unit (NN57-m) and the absence of this geochemical unit from the northern part of the Lesotho magmatic province indicate that these lava flows were emplaced during a previous, geographically limited eruptive phase. However, we have not been able to find any strong evidence for a period of quiescence between the Mafika Lisiu and Moshesh's Ford units, such as thick weathering horizons or paleosols. In any case, the amount of lava emplaced during the first volcanic phase (when the desert environment typical of the Clarens Formation likely continued) appears to be quite small, corresponding to less than 100 m in total thickness, compared to the 650 m emplaced during the second volcanic phase. Confirmation of this suggestion will require a significant number of additional age determinations of the lower part of the volcanic pile. We note that sills intruded in the Karoo sedimentary basin have yielded ages ranging from 184 to 176 Ma [*Encarnacion et al.*, 1996; *Svensen et al.*, 2007; *Jourdan et al.*, 2008]. These ages encompass the two periods of volcanic activity suggested for the Naude's Nek section.

[57] Current geochronological techniques do not allow uncertainties significantly below the 1% level (see above). Paleomagnetic analyses can provide significantly more precise constraints on the rates of volcanic activity. For instance, the mean reversal rate during the Pliensbachian and Toarcian is not precisely known but is generally assumed to be higher than 1 reversal per million years [*Gradstein et al.*, 2004]. The observation of a single reversal in the Naude's Nek section is therefore consistent with a total duration on the order of 1 Myr or even less.

[58] The fact that only 29 individual, distinct magnetic directions were observed in the stratigraphic succession (among which there are 19 directional groups, including from 2 to 10 lava flows each and forming single eruptive events or SEEs, and 10 individual lava flows) implies that the total time of volcanic activity may not have exceeded ~3000 years (29 times 100 years, an upper limit on the emplacement time of a single flow or SEE). This does not include possible quiescence periods between flows corresponding to distinct magnetic directions and hence does not provide the total duration of eruption. The emplacement of huge lava flows may occur in much less than a hundred years, as shown for the Roza flow which erupted in no more than a few years [*Thordarson and Self*, 1998]. Thus the time of eruptive activity may have been as short as a few centuries (i.e., less than 10^{-3} of the total duration). We do not know the volumes of individual lava flows from the Naude's Nek section (contrary to our information for many units in the Deccan of India [*Chenet et al.*, 2008, 2009]), and as a consequence we cannot estimate eruption rates precisely. However, we can use the thicknesses of lava flows (SEEs and individual flow lobes) and their volcanic style to gain some idea on these rates (at least in a relative sense). SEEs represent two thirds of the total lava pile. Only three SEEs, corresponding to DG 24, 27 and 28, reach 70 to 100 m in thickness. The others are on average only about 20 m thick. Thicker lava flows, emplaced as series of inflated pahoehoe sheets, are relatively common in other large igneous provinces, such as the Deccan traps, where mean flow thickness is ~ 40 m [*Chenet et al.*, 2008]. This could be a characteristic feature of the Karoo igneous province, implying smaller flows and flow rates. Additional work on the morphology of lava flows within the Drakensberg Group is required before one can make conclusions about potential differences with other large igneous provinces.

[59] Additional constraints can possibly be derived from the fact that the single reversal recorded in the lava pile corresponds to a rather large number of flows and significant thickness of lava. Several records of reversals in volcanic [*Coe and Prévot*, 1989; *Coe et al.*, 1995; *Herrero-Bervera and Valet*, 1999] or sedimentary rocks [e.g., *Valet et al.*, 1986; *Channell and Lehman*, 1997] display rapid directional changes alternating with periods of standstill. This may imply a secular variation rate during a reversal larger than during stable magnetic polarities [*Valet et al.*, 2008]. We find some evidence of this in our study. We observe a variation in pulse thickness going up section from the base of the transition to the top of the pile (the mean thickness of the DGs increases by a factor 3; Figure 9). This could be due either to an increase in volcanic eruption rate or to a decrease in the amplitude of secular variation, associated with a stronger axial-dipole strength, at the end of the reversal. The 130 m thick lava sequence corresponding to the 10 cooling units (either DGs or individual lava flows) that have recorded the reversal could have been emplaced over a period of volcanic activity as short as a few tens of years. However, the shape and amplitude of the path followed by VGPs during the reversal suggests that much of the total reversal was captured and durations on the order of one to less than ten thousand years [e.g., *Merrill and McFadden*, 1999; *Clement*, 2004; *Valet et al.*, 2008] are more in line with what is generally accepted. Since the total eruption time for the transitional flows may have been much less than 1 kyr and whereas the reversal may have lasted ~5 kyr, most of the elapsed time should correspond to quiescence periods between flows.

[60] A single section, however thick, is clearly not sufficient to outline the eruptive history of the Lesotho remnant of the Karoo CFB. We are currently working on a similar detailed analysis of an even thicker section in the north of Lesotho, the Oxbow section. This should provide access to a record of the full lava pile from earliest to latest flows and evidence for tracing individual SEEs over large distances, as was found to be the case in the Deccan [e.g., *Chenet et al.*, 2009]. We defer more detailed analysis of the "van Zijl" reversal and of the possible connection between Karoo volcanism and the Pliensbachian-Toarcian biotic crises until then.

[61] **Acknowledgments.** This work was supported by Conseil Régional d'Ile de France and the French Ministry of Foreign Affairs in the frame of an ARCUS program with South Africa and by CNRS in the frame of a joint International Program with South Africa entitled !Khure Africa. V.C. is grateful to the South African cochair of !Khure Africa, Maarten de Wit, for continued support. The costs of the geochemical work of J.M. were covered by a grant from the South African National Research Foundation. We thank Rob van der Voo and an anonymous reviewer for helpful comments on the original manuscript. This is IPGP contribution 3146 and Laboratoire de Géochronologie MultiTechniques (LGMT) of UMR IDES contribution 96.

References

Besse, J., and V. Courtillot (2002), Apparent and true polar wander and the geometry of the geomagnetic field over the last 200 Myr, *J. Geophys. Res.*, *107*(B11), 2300, doi:10.1029/2000JB000050.

Bordy, E. M., and O. Catuneanu (2002), Sedimentology and palaeontology of upper Karoo aeolian strata (Early Jurassic) in the Tuli Basin, South Africa, *J. Afr. Earth Sci.*, *35*(2), 301–314, doi:10.1016/S0899-5362(02)00103-3.

Bryan, S. E., I. U. Peate, D. W. Peate, S. Self, D. A. Jerram, M. R. Mawby, J. S. Marsh, and J. A. Miller (2010), The largest volcanic eruptions on Earth, *Earth Sci. Rev.*, *102*(3–4), 207–229, doi:10.1016/j.earscirev.2010.07.001.

Cassignol, C., and P. Y. Gillot (1982), Range and effectiveness of unspiked potassium-argon dating: Experimental groundwork and applications, in *Numerical Dating in Stratigraphy*, edited by G. S. Odin, pp. 159–179, John Wiley, New York.

Cecca, F., and F. Macchioni (2004), The two Early Toarcian (Early Jurassic) extinction events in ammonoids, *Lethaia*, *37*, 35–56, doi:10.1080/00241160310008257.

Channell, J. E. T., and B. Lehman (1997), The last two geomagnetic polarity reversals recorded in high-deposition-rate sediment drifts, *Nature*, *389*(6652), 712–715, doi:10.1038/39570.

Chenet, A. L., X. Quidelleur, F. Fluteau, and V. Courtillot (2007), ^{40}K–^{40}Ar dating of the main Deccan large igneous province: Further evidence of KTB age and short duration, *Earth Planet. Sci. Lett.*, *263*, 1–15, doi:10.1016/j.epsl.2007.07.011.

Chenet, A. L., F. Fluteau, V. Courtillot, M. Gérard, and K. V. Subbarao (2008), Determination of rapid Deccan eruptions across the Cretaceous-Tertiary boundary using paleomagnetic secular variation: Results from a 1200-m-thick section in the Mahabaleshwar escarpment, *J. Geophys. Res.*, *113*, B04101, doi:10.1029/2006JB004635.

Chenet, A. L., V. Courtillot, F. Fluteau, M. Gérard, X. Quidelleur, S. F. R. Khadri, K. V. Subbarao, and T. Thodarson (2009), Determination of rapid Deccan eruptions across the Cretaceous-Tertiary boundary using paleomagnetic secular variation: 2. Constraints from analysis of eight new sections and synthesis for a 3500-m-thick composite section, *J. Geophys. Res.*, *114*, B06103, doi:10.1029/2008JB005644.

Chevallier, L., and A. Woodford (1999), Morpho-tectonics and mechanism of emplacement of the dolerite rings and sills of the western Karoo, South Africa, *S. Afr. J. Geol.*, *102*(1), 43–54.

Clement, B. M. (2004), Dependence of the duration of geomagnetic polarity reversals on site latitude, *Nature*, *428*(6983), 637–640, doi:10.1038/nature02459.

Coe, R. S., and M. Prévot (1989), Evidence suggesting extremely rapid field variation during a geomagnetic reversal, *Earth Planet. Sci. Lett.*, *92*, 292–298, doi:10.1016/0012-821X(89)90053-8.

Coe, R. S., M. Prévot, and P. Camps (1995), New evidence for extraordinarily rapid variation of the geomagnetic field during a reversal, *Nature*, *374*(6524), 687–692, doi:10.1038/374687a0.

Cogné, J. P. (2003), PaleoMac: A MacintoshTM application for treating paleomagnetic data and making plate reconstructions, *Geochem. Geophys. Geosyst.*, *4*(1), 1007, doi:10.1029/2001GC000227.

Cohen, A. S., A. L. Coe, S. M. Harding, and L. Schwark (2004), Osmium isotope evidence for the regulation of atmospheric CO_2 by continental weathering, *Geology*, *32*(2), 157–160, doi:10.1130/G20158.1.

Courtillot, V. (1994), Mass extinctions in the last 300 million years: One impact and seven flood basalts, *Isr. J. Earth Sci.*, *43*, 255–266.

Courtillot, V. E., and P. R. Renne (2003), On the ages of flood basalt events, *C. R. Geosci.*, *335*(1), 113–140, doi:10.1016/S1631-0713(03)00006-3.

Courtillot, V., V. A. Kravchinsky, X. Quidelleur, P. R. Renne, and D. P. Gladkochub (2010), Preliminary dating of the Viluy traps (Eastern Siberia): Eruption at the time of Late Devonian extinction events?, *Earth Planet. Sci. Lett.*, *300*, 239–245, doi:10.1016/j.epsl.2010.09.045.

Cox, K. G. (1988), The Karoo Province, in *Continental Flood Basalts*, edited by I. MacDougall, pp. 239–271, Kluwer Acad., Dordrecht, Netherlands.

Dazé, A., J. K. W. Lee, and M. Villeneuve (2003), An intercalibration study of the Fish Canyon sanidine and biotite $^{40}Ar/^{39}Ar$ standards and some comments on the age of the Fish Canyon Tuff, *Chem. Geol.*, *199*, 111–127, doi:10.1016/S0009-2541(03)00079-2.

Duncan, A. R., R. A. Armstong, A. J. Erlank, J. S. Marsh, and R. T. Watkins (1990), MORB-related dolerites associated with the final phases of Karoo flood basalt volcanism in southern Africa, in *Mafic Dykes and Emplacement Mechanisms*, edited by A. J. Parker, P. C. Rickwood, and D. H. Tucker, pp. 119–129, A. A. Balkema, Rotterdam, Netherlands.

Duncan, R. A., R. P. Hooper, J. Rehacek, J. S. Marsh, and A. R. Duncan (1997), The timing and duration of the Karoo igneous event, southern Gondwana, *J. Geophys. Res.*, *102*, 18,127–18,138, doi:10.1029/97JB00972.

Eales, H. V., J. S. Marsh, and K. G. Cox (1984), The Karoo Igneous Province: An introduction, in *Petrogenesis of the Volcanic Rocks of the Karoo Province*, edited by A. J. Erlank, *Spec. Publ. Geol. Soc. S. Afr.*, *13*, 1–26.

Elliot, D. H., and T. H. Fleming (2000), Weddell triple junction: The principal focus of Ferrar and Karoo magmatism during initial breakup of Gondwana, *Geology*, *28*(6), 539–542, doi:10.1130/0091-7613(2000)28<539:WTJTPF>2.0.CO;2.

Encarnacion, J., T. H. Fleming, D. H. Elliot, and H. V. Eales (1996), Synchronous emplacement of Ferrar and Karoo dolerites and the early breakup of Gondwana, *Geology*, *24*(6), 535–538, doi:10.1130/0091-7613(1996)024<0535:SEOFAK>2.3.CO;2.

Fiet, N., X. Quidelleur, O. Parize, L. G. Bulot, and P. Y. Gillot (2006), Lower Cretaceous stage durations combining radiometric data and orbital chronology: Towards a more stable relative time scale?, *Earth Planet. Sci. Lett.*, *246*, 407–417, doi:10.1016/j.epsl.2006.04.014.

Fisher, R. A. (1953), Dispersion on a sphere, *Proc. R. Soc. London, A*, *217*, 295–305, doi:10.1098/rspa.1953.0064.

Gallet, Y., A. Genevey, and M. Le Goff (2002), Three millennia of directional variation of the Earth's magnetic field in western Europe as revealed by archeological artefacts, *Phys. Earth Planet. Inter.*, *131*(1), 81–89, doi:10.1016/S0031-9201(02)00030-4.

Gallet, Y., A. Genevey, and V. Courtillot (2003), On the possible occurrence of 'archaeomagnetic jerks' in the geomagnetic field over the past three millennia, *Earth Planet. Sci. Lett.*, *214*, 237–242, doi:10.1016/S0012-821X(03)00362-5.

Ganino, C., and N. T. Arndt (2009), Climate changes caused by degassing of sediments during the emplacement of large igneous provinces, *Geology*, *37*(4), 323–326, doi:10.1130/G25325A.1.

Gillot, P. Y., and Y. Cornette (1986), The Cassignol technique for potassium-argon dating, precision and accuracy: Examples from late Pleistocene to recent volcanics from southern Italy, *Chem. Geol.*, *59*, 205–222.

Gradstein, F. M., J. G. Ogg, and A. G. Smith (2004), *A Geologic Time Scale 2004*, 589 pp., Cambridge Univ. Press, Cambridge, U. K.

Graham, K. W. T., and A. L. Hales (1957), Palaeomagnetic measurements on Karroo dolerites, *Adv. Phys.*, *6*(22), 149–161, doi:10.1080/00018739700101511.

Green, D. (1966), The Karroo System in Bechuanaland, *Bull. 2*, 74 pp., Geol. Surv. of Bechuanaland, Gaborone, Botswana.

Guilbaud, M. N., S. Self, T. Thordarson, and S. Blake (2005), Morphology, surface structures, and emplacement of lavas produced by Laki, A.D. 1783–1784, *Spec. Pap. Geol. Soc. Am.*, *396*, 81–102.

Hargraves, R. B., J. Rehacek, and P. R. Hooper (1997), Palaeomagnetism of the Karoo igneous rocks in southern Africa, *S. Afr. J. Geol.*, *100*(3), 195–212.

Harris, C., J. S. Marsh, A. R. Duncan, and A. J. Erlank (1990), The petrogenesis of the Kirwan Basalts of Dronning Maud Land, Antarctica, *J. Petrol.*, *31*, 341–369.

Hergt, J. M., B. W. Chappell, M. T. McCulloch, I. McDougall, and A. R. Chivas (1989), Geochemical and isotopic constraints on the origin of the Jurassic dolerites of Tasmania, *J. Petrol.*, *30*, 841–883.

Hergt, J. M., D. W. Peate, and C. J. Hawkesworth (1991), The petrogenesis of Mesozoic Gondwana low-Ti flood basalts, *Earth Planet. Sci. Lett.*, *105*, 134–148, doi:10.1016/0012-821X(91)90126-3.

Hermoso, M., F. Minoletti, L. Le Callonnec, H. C. Jenkyns, S. P. Hesselbo, R. E. M. Rickaby, M. Renard, M. de Rafélis, and L. Emmanuel (2009), Global and local forcing of Early Toarcian seawater chemistry: A comparative study of different paleoceanographic settings (Paris and Lusitanian basins), *Paleoceanography*, *24*, PA4208, doi:10.1029/2009PA001764.

Herrero-Bervera, E., and J. P. Valet (1999), Paleosecular variation during sequential geomagnetic reversals from Hawaii, *Earth Planet. Sci. Lett.*, *171*, 139–148, doi:10.1016/S0012-821X(99)00145-4.

Hesselbo, S. P., D. R. Gröcke, H. C. Jenkyns, C. J. Bjerrum, P. Farrimond, H. S. Morgans Bell, and O. R. Green (2000), Massive dissociation of gas hydrate during a Jurassic oceanic event, *Nature*, *406*(6794), 392–395, doi:10.1038/35019044.

Hofmann, C., G. Féraud, and V. Courtillot (2000), $^{40}Ar/^{39}Ar$ dating of mineral separates and whole rocks from the Western Ghats lava pile: Further constraints on duration and age of the Deccan traps, *Earth Planet. Sci. Lett.*, *180*, 13–27, doi:10.1016/S0012-821X(00)00159-X.

Holzforster, F. (2007), Lithology and depositional environments of the Lower Jurassic Clarens Formation in the eastern Cape, South Africa, *S. Afr. J. Geol.*, *110*(4), 543–560, doi:10.2113/gssajg.110.4.543.

Hulot, G., and J. L. Le Mouël (1994), A statistical approach to the Earth's main magnetic field, *Phys. Earth Planet. Inter.*, *82*(3–4), 167–183, doi:10.1016/0031-9201(94)90070-1.

Ivanov, A. V., S. V. Rasskazov, G. D. Feoktistov, H. He, and A. Boven (2005), $^{40}Ar/^{39}Ar$ dating of Usol'skii sill in the south-eastern Siberian Traps Large Igneous Province: Evidence for long-lived magmatism, *Terra Nova*, *17*(3), 203–208, doi:10.1111/j.1365-3121.2004.00588.x.

Jarboe, N. A., R. S. Coe, P. R. Renne, J. M. G. Glen, and E. A. Mankinen (2008), Quickly erupted volcanic sections of the Steens Basalt, Columbia

River Basalt Group: Secular variation, tectonic rotation, and the Steens Mountain reversal, *Geochem. Geophys. Geosyst.*, *9*, Q11010, doi:10.1029/2008GC002067.

Jenkyns, H. C. (1988), The early Toarcian (Jurassic) event: Stratigraphy, sedimentary and geochemical evidence, *Am. J. Sci.*, *288*, 101–151, doi:10.2475/ajs.288.2.101.

Jerram, D. A., and M. Widdowson (2005), The anatomy of Continental Flood Basalt Provinces: Geological constraints on the processes and products of flood volcanism, *Lithos*, *79*(3–4), 385–405, doi:10.1016/j.lithos.2004.09.009.

Johnson, M. R., C. J. VanVuuren, W. F. Hegenberger, R. Key, and U. Shoko (1996), Stratigraphy of the Karoo Supergroup in southern Africa: An overview, *J. Afr. Earth Sci.*, *23*(1), 3–15, doi:10.1016/S0899-5362(96)00048-6.

Johnson, M. R., C. J. V. Vuuren, J. N. J. Visser, D. I. Cole, H. D. V. Wickens, A. D. M. Christie, and D. L. Roberts (1997), The Foreland Karoo Basin, South Africa, in *African Basins: Sedimentary Basins of the World*, edited by R. C. Selley, chap. 12, pp. 269–317, Elsevier, Amsterdam.

Jones, D. L., R. A. Duncan, J. C. Briden, D. E. Randall, and C. MacNiocaill (2001), Age of the Batoka basalts, northern Zimbabwe, and the duration of Karoo large igneous province magmatism, *Geochem. Geophys. Geosyst.*, *2*(2), 1022, doi:10.1029/2000GC000110.

Jourdan, F., G. Féraud, H. Bertrand, A. B. Kampunzu, G. Tshoso, B. L. Gall, J. J. Tiercelin, and P. Capiez (2004), The Karoo triple junction questioned: Evidence from $^{40}Ar/^{39}Ar$ Jurassic and Proterozoic ages and geochemistry of the Okavango dike swarm (Botswana), *Earth Planet. Sci. Lett.*, *222*, 989–1006, doi:10.1016/j.epsl.2004.03.017.

Jourdan, F., G. Féraud, H. Bertrand, A. B. Kampunzu, G. Tshoso, M. K. Watkeys, and B. L. Gall (2005), The Karoo large igneous province: Brevity, origin, and relation with mass extinction questioned by new $^{40}Ar/^{39}Ar$ age data, *Geology*, *33*(9), 745–748, doi:10.1130/G21632.1.

Jourdan, F., G. Féraud, H. Bertrand, M. K. Watkeys, A. B. Kampunzu, and B. Le Gall (2006), Basement control on dyke distribution in Large Igneous Provinces: Case study of the Karoo triple junction, *Earth Planet. Sci. Lett.*, *241*, 307–322, doi:10.1016/j.epsl.2005.10.003.

Jourdan, F., G. Féraud, H. Bertrand, and M. K. Watkeys (2007a), From flood basalts to the inception of oceanization: Example from the $^{40}Ar/^{39}Ar$ high-resolution picture of the Karoo large igneous province, *Geochem. Geophys. Geosyst.*, *8*, Q02002, doi:10.1029/2006GC001392.

Jourdan, F., G. Féraud, H. Bertrand, M. K. Watkeys, and P. R. Renne (2007b), Distinct brief major events in the Karoo large igneous province clarified by new $^{40}Ar/^{39}Ar$ ages on the Lesotho basalts, *Lithos*, *98*(1–4), 195–209, doi:10.1016/j.lithos.2007.03.002.

Jourdan, F., G. Féraud, H. Bertrand, M. K. Watkeys, and P. R. Renne (2008), The $^{40}Ar/^{39}Ar$ ages of the sill complex of the Karoo large igneous province: Implications for the Pliensbachian-Toarcian climate change, *Geochem. Geophys. Geosyst.*, *9*, Q06009, doi:10.1029/2008GC001994.

Kirschvink, J. L. (1980), The least squares line and plane and the analysis of palaeomagnetic data, *Geophys. J. R. Astron. Soc.*, *62*, 699–718.

Knight, K. B., S. Nomade, P. R. Renne, A. Marzoli, H. Bertrand, and N. Youbi (2004), The Central Atlantic Magmatic Province at the Triassic-Jurassic boundary: Paleomagnetic and $^{40}Ar/^{39}Ar$ evidence from Morocco for brief, episodic volcanism, *Earth Planet. Sci. Lett.*, *228*, 143–160, doi:10.1016/j.epsl.2004.09.022.

Knoll, F. (2005), The tetrapod fauna of the Upper Elliot and Clarens formations in the main Karoo Basin (South Africa and Lesotho), *Bull. Soc. Geol. Fr.*, *176*(1), 81–91, doi:10.2113/176.1.81.

Kosterov, A. A., and M. Perrin (1996), Paleomagnetism of the Lesotho basalt, southern Africa, *Earth Planet. Sci. Lett.*, *139*, 63–78, doi:10.1016/0012-821X(96)00005-2.

Kravchinsky, V. A., K. M. Konstantinov, V. Courtillot, J. I. Savrasov, J. P. Valet, S. Chernyi, S. Mishenin, and B. Parasotka (2002), Paleomagnetism of East Siberian Traps and kimberlites: Two new poles and paleogeographic reconstructions at about 360 and 250 Ma, *Geophys. J. Int.*, *148*, 1–33, doi:10.1046/j.0956-540x.2001.01548.x.

Kuiper, K. F., F. J. Hilgen, J. Steenbrink, and J. R. Wijbrans (2004), $^{40}Ar/^{39}Ar$ ages of tephras intercalated in astronomically tuned Neogene sedimentary sequences in the eastern Mediterranean, *Earth Planet. Sci. Lett.*, *222*, 583–597, doi:10.1016/j.epsl.2004.03.005.

Kuiper, K. F., A. Deino, F. J. Hilgen, W. Krijgsman, P. R. Renne, and J. R. Wijbrans (2008), Synchronizing rock clocks of Earth history, *Science*, *320*(5875), 500–504, doi:10.1126/science.1154339.

Kyle, P. R., D. H. Elliot, and J. F. Sutter (1981), Jurassic Ferrar Supergroup tholeiites from the Transantarctic Mountains, Antarctica, and their relationship to the initial fragmentation of Gondwana, in *Gondwana Five: Proceedings of the Fifth International Gondwana Symposium*, edited by M. M. Cresswell and P. Vella, pp. 283–287, Balkema, Rotterdam, Netherlands.

Lanphere, M. A., and H. Baadsgaard (2001), Precise K-Ar, $^{40}Ar/^{39}Ar$, Rb-Sr and U/Pb mineral ages from the 27.5 Ma Fish Canyon Tuff reference standard, *Chem. Geol.*, *175*, 653–671, doi:10.1016/S0009-2541(00)00291-6.

Le Gall, B., G. Tshoso, F. Jourdan, G. Féraud, H. Bertrand, J. J. Tiercelin, A. B. Kampunzu, M. P. Modisi, J. Dyment, and M. Maia (2002), $^{40}Ar/^{39}Ar$ geochronology and structural data from the giant Okavango and related mafic dyke swarms, Karoo igneous province, northern Botswana, *Earth Planet. Sci. Lett.*, *202*, 595–606, doi:10.1016/S0012-821X(02)00763-X.

Little, C. T. S. (1996), The Pliensbachian-Toarcian (Lower Jurassic) extinction event, in *The Cretaceous-Tertiary Event and Other Catastrophes in Earth History*, edited by G. Ryder, D. Fastovsky, and S. Gartner, *Spec. Pap. Geol. Soc. Am.*, *307*, 505–512.

Little, C. T. S., and M. J. Benton (1995), Early Jurassic mass extinction: A global long term event, *Geology*, *23*(6), 495–498, doi:10.1130/0091-7613(1995)023<0495:EJMEAG>2.3.CO;2.

Lock, B. E., A. L. Paverd, and T. J. Broderick (1974), Stratigraphy of the Karroo volcanic rocks of the Barkly East district, *Trans. Geol. Soc. S. Afr.*, *77*, 117–129.

Mankinen, E. A., M. Prévot, C. S. Grommé, and R. S. Coe (1985), The Steens mountain (Oregon) geomagnetic polarity transition: 1. Directional variation, duration of episodes, and rock magnetism, *J. Geophys. Res.*, *90*, 10,393–10,416, doi:10.1029/JB090iB12p10393.

Marsh, J. S., and H. V. Eales (1984), The chemistry and petrogenesis of igneous rocks of the Karoo central area, southern Africa, in *Petrogenesis of the Volcanic Rocks of the Karoo Province*, edited by A. J. Erlank, *Spec. Publ. Geol. Soc. S. Afr.*, *13*, 27–68.

Marsh, J. S., P. R. Hooper, J. Rehacek, A. R. Duncan, and R. A. Duncan (1997), Stratigraphy and age of Karoo basalts of Lesotho and implications for correlation within the Karoo Igneous Province, in *Large Igneous Provinces*, *Geophys. Monogr. Ser.*, vol. 100, edited by J. J. Mahoney and M. Coffin, pp. 247–272, AGU, Washington, D. C.

Marsh, J. S., R. S. Swart, and D. Phillips (2003), Implications of a new $^{40}Ar/^{39}Ar$ age for a basalt flow interbedded with the Etjo Formation, Northeast Namibia, *S. Afr. J. Geol.*, *106*(4), 281–286, doi:10.2113/106.4.281.

McClintock, M., J. S. Marsh, and J. D. L. White (2008), Compositionally diverse magmas erupted close together in space and time within a Karoo flood basalt crater complex, *Bull. Volcanol.*, *70*, 923–946, doi:10.1007/s00445-007-0178-6.

McElhinny, M. W., and R. T. Merrill (1975), Geomagnetic secular variation over the past 5 m.y., *Rev. Geophys.*, *13*, 687–708, doi:10.1029/RG013i005p00687.

McElwain, J., J. Wade-Murphy, and S. P. Hesselbo (2005), Changes in carbon dioxide during an oceanic anoxic event linked to intrusion into Gondwana coals, *Nature*, *435*(7041), 479–482, doi:10.1038/nature03618.

McFadden, P. L., and F. J. Lowes (1981), The discrimination of mean directions drawn from Fisher distributions, *Geophys. J. R. Astron. Soc.*, *67*, 19–33.

McFadden, P. L., and M. W. McElhinny (1988), The combined analysis of remagnetization circles and direct observations in palaeomagnetism, *Earth Planet. Sci. Lett.*, *87*, 161–172, doi:10.1016/0012-821X(88)90072-6.

McFadden, P. L., and M. W. McElhinny (1990), Classification of the reversal test in paleomagnetism, *Geophys. J. Int.*, *103*, 725–729, doi:10.1111/j.1365-246X.1990.tb05683.x.

McFadden, P. L., R. T. Merrill, M. W. McElhinny, and S. Lee (1991), Reversals of the Earth's magnetic field and temporal variations of the dynamo families, *J. Geophys. Res.*, *96*, 3923–3933, doi:10.1029/90JB02275.

Merrill, R. T., and P. L. McFadden (1999), Geomagnetic polarity transitions, *Rev. Geophys.*, *37*, 201–226, doi:10.1029/1998RG900004.

Mitchell, A. A., V. R. Ramluckan, J. N. Dunlevey, and B. M. Eglington (1996), The basalt stratigraphy of the Sani Pass, Kwazulu/Natal Drakensberg, *S. Afr. J. Geol.*, *99*(3), 251–262.

Mitchell, C., R. M. Ellam, and K. G. Cox (1999), Mesozoic dolerite dykes of the Falkland Islands: Petrology, petrogenesis and implications for geochemical provinciality in Gondwanaland low-Ti basaltic rocks, *J. Geol. Soc.*, *156*, 901–916, doi:10.1144/gsjgs.156.5.0901.

Mortimer, N., D. Parkinson, J. I. Raine, C. J. Adams, I. J. Graham, P. J. Oliver, and K. Palmer (1995), Ferrar magmatic province rocks discovered in New Zealand: Implications for Mesozoic Gondwana geology, *Geology*, *23*(2), 185–188, doi:10.1130/0091-7613(1995)023<0185:FMPRDI>2.3.CO;2.

Odin, G. S., et al. (1982), Interlaboratory standards for dating purposes, in *Numerical Dating in Stratigraphy*, edited by G. S. Odin, pp. 123–150, John Wiley, Chichester, U. K.

Ogg, J. G., and A. G. Smith (2004), The geomagnetic polarity time scale, in *A Geologic Time Scale 2004*, edited by F. M. Gradstein, J. G. Ogg, and A. B. Smith, pp. 63–86, Cambridge Univ. Press, Cambridge, U. K.

Ogg, J. G., G. Ogg, and F. M. Gradstein (2008), *The Concise Geologic Time Scale*, 77 pp., Cambridge Univ. Press, Cambridge, U. K.

Pálfy, J., and P. L. Smith (2000), Synchrony between Early Jurassic extinction, oceanic anoxic event, and the Karoo-Ferrar flood basalt volcanism, *Geology*, *28*(8), 747–750, doi:10.1130/0091-7613(2000)28<747:SBEJEO>2.0.CO;2.

Pavlov, V., F. Fluteau, R. Veselovsky, and A. Fetisova (2010), Geomagnetic secular variations and volcanic pulses in the Siberian traps, *Geophys. Res. Abstr.*, *12*, Abstract EGU2010-5872.

Prévot, M., N. Roberts, J. Thompson, L. Faynot, M. Perrin, and P. Camps (2003), Revisiting the Jurassic geomagnetic reversal recorded in the Lesotho Basalt (southern Africa), *Geophys. J. Int.*, *155*, 367–378, doi:10.1046/j.1365-246X.2003.02029.x.

Quidelleur, X., P. Y. Gillot, V. Soler, and J. C. Lefevre (2001), K/Ar dating extended into the last millennium: Application to the youngest effusive episode of the Teide volcano (Spain), *Geophys. Res. Lett.*, *28*, 3067–3070, doi:10.1029/2000GL012821.

Rampino, M. R., and R. B. Stothers (1988), Flood basalt volcanism during the past 250 million years, *Science*, *241*(4866), 663–668, doi:10.1126/science.241.4866.663.

Rehacek, J. (1995), Chemical and paleomagnetic stratigraphy of basalts in Northern Lesotho, Karoo Province, Ph.D. thesis, 298 pp., Dep. of Geol., Wash. State Univ., Pullman.

Renne, P. R., A. L. Deino, R. C. Walter, B. D. Turrin, C. C. Swisher, T. A. Becker, G. H. Curtis, W. D. Sharp, and A. R. Jaouni (1994), Intercalibration of astronomical and radioisotopic time, *Geology*, *22*(9), 783–786, doi:10.1130/0091-7613(1994)022<0783:IOAART>2.3.CO;2.

Renne, P. R., C. C. Swisher, A. L. Deino, D. B. Karner, T. L. Owens, and D. J. de Paolo (1998), Intercalibration of standards, absolute ages and uncertainties in $^{40}Ar/^{39}Ar$ dating, *Chem. Geol.*, *145*, 117–152, doi:10.1016/S0009-2541(97)00159-9.

Renne, P. R., R. Mundil, G. Balco, K. Min, and K. R. Ludwig (2010), Joint determination of ^{40}K decay constants and $^{40}Ar^*/^{40}K$ for the Fish Canyon sanidine standard, and improved accuracy for $^{40}Ar/^{39}Ar$ geochronology, *Geochim. Cosmochim. Acta*, *74*, 5349–5367, doi:10.1016/j.gca.2010.06.017.

Riisager, P., J. Riisager, N. Abrahamsen, and R. Waagstein (2002), New paleomagnetic pole and magnetostratigraphy of Faroe Islands flood volcanics, North Atlantic igneous province, *Earth Planet. Sci. Lett.*, *201*, 261–276, doi:10.1016/S0012-821X(02)00720-3.

Riisager, J., P. Riisager, and A. K. Pedersen (2003), Paleomagnetism of large igneous provinces: Case-study from West Greenland, North Atlantic igneous province, *Earth Planet. Sci. Lett.*, *214*, 409–425, doi:10.1016/S0012-821X(03)00367-4.

Riley, T. R., and K. B. Knight (2001), Age of pre-break-up Gondwana magmatism, *Antarct. Sci.*, *13*(2), 99–110, doi:10.1017/S0954102001000177.

Riley, T. R., I. L. Millar, M. K. Watkeys, M. L. Curtis, P. T. Leat, M. B. Klausen, and C. M. Fanning (2004), U-Pb zircon (SHRIMP) ages for the Lebombo rhyolites, South Africa: Refining the duration of Karoo volcanism, *J. Geol. Soc.*, *161*(4), 547–550, doi:10.1144/0016-764903-181.

Riley, T. R., P. T. Leat, M. L. Curtis, I. L. Millar, R. A. Duncan, and A. Fazel (2005), Early Middle Jurassic dolerite dykes from Western Dronning Maud Land (Antarctica): Identifying mantle sources in the Karoo Large Igneous Province, *J. Petrol.*, *46*, 1489–1524, doi:10.1093/petrology/egi023.

Riley, T. R., M. L. Curtis, P. T. Leat, M. K. Watkeys, A. R. Duncan, I. L. Millar, and W. H. Owens (2006), Overlap of Karoo and Ferrar magma Types in KwaZulu-Natal, South Africa, *J. Petrol.*, *47*, 541–566, doi:10.1093/petrology/egi085.

Rodriguez, E., C. S. Morris, J. Belz, E. Chapin, J. Martin, W. Daffer, and S. Hensley (2005), An assessment of the SRTM topographic products, *Tech. Rep. JPL D-31639*, 143 pp., Jet Propul. Lab., Pasadena, Calif.

Self, S., T. Thordarson, and L. P. Keszthelyi (1997), Emplacement of continental flood basalt lava flows, in *Large Igneous Provinces: Continental, Oceanic, and Planetary Flood Volcanism*, *Geophys. Monogr. Ser.*, vol. 100, edited by J. Mahoney and M. F. Coffin, pp. 381–410, AGU, Washington, D. C.

Self, S., M. Widdowson, T. Thordarson, and A. E. Jay (2006), Volatile fluxes during flood basalt eruptions and potential effects on the global environment: A Deccan perspective, *Earth Planet. Sci. Lett.*, *248*, 518–532.

Smith, R. M. H. (1990), A review of stratigraphy and sedimentary environments of the Karoo Basin of South Africa, *J. Afr. Earth Sci.*, *10*(1–2), 117–137, doi:10.1016/0899-5362(90)90050-O.

Smith, R. M. H. (1993), Vertebrate taphonomy of Late Permian floodplain deposits in the southwestern Karoo Basin of South Africa, *Palaios*, *8*, 45–67, doi:10.2307/3515221.

Smith, R. M. H., B. P. Turner, P. J. Hancox, B. R. Rubidge, and O. Catuneanu (1998), Trans-Karoo II: 100 million years of changing terrestrial environments in the main Karoo basin, in *Guidebook Gondwana: 10th International Conference*, 117 pp., Univ. of Cape Town, Cape Town, South Africa.

Spell, T. L., and I. McDougall (2003), Characterization and calibration of $^{40}Ar/^{39}Ar$ dating standards, *Chem. Geol.*, *198*, 189–211, doi:10.1016/S0009-2541(03)00005-6.

Steiger, R. H., and E. Jäger (1977), Subcommission on geochronology: Convention on the use of decay constants in geo and cosmochronology, *Earth Planet. Sci. Lett.*, *36*, 359–362, doi:10.1016/0012-821X(77)90060-7.

Storey, B. C., P. T. Leat, and J. K. Ferris (2001), The location of mantle-plume centers during the initial stages of Gondwana breakup, in *Mantle Plumes: Their Identification Through Time*, edited by R. E. Ernst and K. L. Buchan, *Spec. Pap. Geol. Soc. Am.*, *352*, 71–80, doi:10.1130/0-8137-2352-3.71.

Suan, G., E. Mattioli, B. Pittet, S. Mailliot, and C. Lécuyer (2008), Evidence for major environmental perturbation prior to and during the Toarcian (Early Jurassic) Oceanic Anoxic Event from the Lusitanian Basin, Portugal, *Paleoceanography*, *23*, PA1202, doi:10.1029/2007PA001459.

Suan, G., E. Mattioli, B. Pittet, C. Lécuyer, B. Suchéras-Marx, L. V. Duarte, M. Philippe, L. Reggiani, and F. Martineau (2010), Secular environmental precursors to Early Toarcian (Jurassic) extreme climate changes, *Earth Planet. Sci. Lett.*, *290*, 448–458, doi:10.1016/j.epsl.2009.12.047.

Svensen, H., S. Planke, A. Malthe-Sörenssen, B. Jamtveit, R. Myklebust, T. Rasmussen Eidem, and S. S. Rey (2004), Release of methane from a volcanic basin as a mechanism for initial Eocene global warming, *Nature*, *429*(6991), 542–545, doi:10.1038/nature02566.

Svensen, H., S. Planke, L. Chevallier, A. Malthe-Sörenssen, F. Corfu, and B. R. Jamtveit (2007), Hydrothermal venting of greenhouse gases triggering Early Jurassic global warming, *Earth Planet. Sci. Lett.*, *256*, 554–566, doi:10.1016/j.epsl.2007.02.013.

Thiede, D. S., and P. M. Vasconcelos (2010), Parana flood basalts: Rapid extrusion hypothesis confirmed by new Ar-40/Ar-39 results, *Geology*, *38*(8), 747–750, doi:10.1130/G30919.1.

Thompson, R. N., S. A. Gibson, A. P. Dickin, and P. M. Smith (2001), Early Cretaceous basalt and picrite dykes of the southern Etendeka Region, NW Namibia: Windows into the role of the Tristan Mantle Plume in Parana, Etendeka magmatism, *J. Petrol.*, *42*, 2049–2081, doi:10.1093/petrology/42.11.2049.

Thordarson, T., and S. Self (1998), The Roza Member, Columbia River Basalt Group: A gigantic pahoehoe lava flow field formed by endogenous processes?, *J. Geophys. Res.*, *103*, 27,411–27,445, doi:10.1029/98JB01355.

Turner, G., J. C. Huneke, F. A. Podosek, and G. J. Wasserburg (1971), ^{40}Ar-^{39}Ar ages and cosmic ray exposure ages of Apollo 14 samples, *Earth Planet. Sci. Lett.*, *12*, 19–35, doi:10.1016/0012-821X(71)90051-3.

Valet, J. P., C. Laj, and P. Tucholka (1986), High-resolution sedimentary record of a geomagnetic reversal, *Nature*, *322*(6074), 27–32, doi:10.1038/322027a0.

Valet, J. P., G. Plenier, and E. Herrero-Bervera (2008), Geomagnetic excursions reflect an aborted polarity state, *Earth Planet. Sci. Lett.*, *274*, 472–478, doi:10.1016/j.epsl.2008.07.056.

Vandamme, D. (1994), A new method to determine paleosecular variation, *Phys. Earth Planet. Inter.*, *85*(1–2), 131–142, doi:10.1016/0031-9201(94)90012-4.

Vandamme, D., V. Courtillot, J. Besse, and R. Montigny (1991), Paleomagnetism and age determinations of the Deccan Traps (India): Results of a Nagpur-Bombay Traverse and review of earlier work, *Rev. Geophys.*, *29*, 159–190, doi:10.1029/91RG00218.

Van Zijl, J. S. V., K. W. T. Graham, and A. L. Hales (1962a), The palaeomagnetism of the Stormberg lavas of South Africa 1: Evidence for a genuine reversal of the Earth's field in Triassic-Jurassic times, *Geophys. J. R. Astron. Soc.*, *7*, 23–39.

Van Zijl, J. S. V., K. W. T. Graham, and A. L. Hales (1962b), The palaeomagnetism of the Stormberg lavas of South Africa 2: The behaviour of the magnetic field during a reversal, *Geophys. J. R. Astron. Soc.*, *7*, 169–182.

Wignall, P. B. (2001), Large igneous provinces and mass extinctions, *Earth Sci. Rev.*, *53*(1–2), 1–33, doi:10.1016/S0012-8252(00)00037-4.

Wignall, P. B., and D. P. G. Bond (2008), The end-Triassic and Early Jurassic mass extinction records in the British Isles, *Proc. Geol. Assoc.*, *119*, 73–84.

Wignall, P. B., et al. (2009), Mass extinction, and carbon isotope fluctuations in the Middle Permian of China, *Science*, *324*(5931), 1179–1182, doi:10.1126/science.1171956.

Zijderveld, J. D. A. (1967), Demagnetization rock-analysis of results, in *Methods in Paleomagnetism*, edited by D. W. Collinson, K. M. Creer, and S. K. Runcorn, pp. 254–286, Elsevier, Amsterdam.

V. Courtillot, F. Fluteau, and M. Moulin, Equipe de Paléomagnétisme, Institut de Physique du Globe, UMR 7154, Sorbonne Paris Cité, F-75005 Paris, France. (mmoulin@ipgp.fr)

G. Delpech and X. Quidelleur, Laboratoire IDES, UMR 8148, Université Paris-Sud, F-91405 Paris, France.

M. Gérard, IMPMC, IRD, UMR 7590, UPMC, IPGP, CNRS, Campus Jussieu, F-75252 Paris, France.

A. E. Jay, Department of Earth Science and Engineering, South Kensington Campus, Imperial College, London SW7 2AZ, UK.

J. Marsh, Department of Geology, Rhodes University, PO Box 94, Grahamstown 6140, South Africa.